

# Hydrodynamic modelling of proposed expansion of the Port of Tauranga shipping channels and wharves

---

2018

ERI report number 119

Prepared for the Port of Tauranga Ltd

Julia C. Mullarney and Willem P. de Lange

Environmental Research Institute  
Faculty of Science and Engineering  
The University of Waikato, Private Bag 3105  
Hamilton, New Zealand



THE UNIVERSITY OF  
**WAIKATO**  
*Te Whare Wānanga o Waikato*

**Cite report as:**

Mullarney, J.C & de Lange, W.P., 2018. Hydrodynamic modelling of proposed expansion of the Port of Tauranga shipping channels and wharves. *Environmental Research Institute Report No 119*. Client report prepared for Port of Tauranga. Environmental Research Institute, Faculty of Science and Engineering, The University of Waikato, Hamilton. 30 pp.

*Reviewed by:*



Professor Karin Bryan  
School of Science  
University of Waikato

*Approved for release by:*



Dr John Tyrell  
Acting Director  
Environmental Research Institute  
University of Waikato

## Table of Contents

<b>Table of figures</b>	<b>1</b>
<b>Table of tables</b>	<b>3</b>
<b>Executive Summary</b>	<b>4</b>
<b>Introduction</b>	<b>5</b>
<b>Field observations</b>	<b>7</b>
<b>Numerical modelling</b>	<b>8</b>
<b>Model calibration</b>	<b>10</b>
<b>Validation results</b>	<b>13</b>
<b>Model scenarios</b>	<b>14</b>
<i>Results from scenario simulations: Comparison between the base run (present conditions) and future development model</i>	15
<i>Results from scenario simulations: Comparison between present (base run) and former (pre-2016 dredging) bathymetries.</i>	19
<b>Conclusions</b>	<b>20</b>
<b>References</b>	<b>21</b>
<b>Appendix One – Calibration plots (PUV)</b>	<b>23</b>

## Table of Figures

Figure 1. Proposed extensions to the Mount Maunganui and Suphur Point Wharves, and Stella Passage shipping channel under the Port of Tauranga Ltd Stella Development Plan.	5
Figure 2. Locations within the southeastern basin of Tauranga Harbour: (A) main components of the tidal inlet system (ETD and FTD are the ebb tidal delta and flood tidal delta respectively); and (B) main components of Stella Passage and the upper harbour. From Figures 2.2 & 2.3 of Watson (2016).	6
Figure 3. Google Earth image showing locations of instruments deployed during the field experiment undertaken in March and April 2017. Circles indicate Acoustic Doppler (Current) Profilers (ADCPs) and squares show Acoustic Doppler Velocimeters (ADVs)	7
Figure 4. Numerical grid of the southern Tauranga Harbour. Grid resolution was 40, 20 and 80 m in the light grey, black, and dark grey domains, respectively. Domain decomposition boundaries between grids are shown in blue. Open boundaries at which forcing is applied are shown in red.	9
Figure 5: Model bathymetry. The colour bar on the right shows depth in metres.	9
Figure 6. Pressure time series from site #1 (outside the harbour). Sections of the time series used for calibration and validation are shown in thick solid and thick dashed lines, respectively.	11
Figure 7: Spatially varying bottom roughness map used in calibrated model. The colour bar shows the Chézy coefficient ( $m^{1/2} s^{-1}$ ).	12
Figure 8. Bathymetries for all modelled scenarios for development of the Port of Tauranga. The colour bar shows depth in m: (a) Base run; (b) pre-2016 dredging; and (c) future development model. In (c), the black lines show the approximate location of the thin dams representing land reclamation and wharf extensions.	14
Figure 9. Precise grid locations of thin dams (thick red lines) used in the future development model to represent land reclamation and wharf extensions.	15
Figure 10. Water levels during neap tide for location closest to port developments (#9) for modelling scenarios base run (black line) and future development model (red dot-dash line). High and low tide are enlarged to highlight deviations affecting the tidal range.	16

Figure 11. Water levels during spring tide for location closest to port developments (#9) for modelling scenarios base run (black line) and future development model (red dot-dash line). High and low tide are enlarged to highlight deviations affecting the tidal range.	16
Figure 12. Differences in flow speeds in $m.s^{-1}$ between base run and future development model. Differences at times closest (<30 mins from) to peak flood (a) and peak ebb (b) during neap tides. The colour bar indicates the velocity difference in $m.s^{-1}$ , with positive values corresponding to a reduction in velocity.	17
Figure 13. Differences in flow speeds in $m.s^{-1}$ between base run and future development model. Differences at times closest (<30 mins from) to peak flood (a) and peak ebb (b) during spring tides. The colour bar indicates the velocity difference in $m.s^{-1}$ , with positive values corresponding to a reduction in velocity.	17
Figure 14. Close up showing predicted differences in flow speeds in $m.s^{-1}$ between base run and future development model in area around the Port of Tauranga. Differences at times closest (<30 mins from) to peak flood (a) and peak ebb (b) during spring tides. The colour bar indicates the velocity difference in $m.s^{-1}$ , with positive values corresponding to a reduction in velocity.	17
Figure 15. Velocity vectors during neap tides in the area of proposed port developments. Results from times closest (<30 mins from) to peak flood tide (a and b) and peak ebb tide (panels c and d). The left-hand column (a and c) shows the base run and the right-hand column (b and d) shows results from the future development model. The colour bar shows the horizontal depth-averaged current speeds ( $m.s^{-1}$ ).	18
Figure 16. Velocity vectors during spring tides in the area of proposed port developments. Results from times closest (<30 mins from) to peak flood tide (a and b) and peak ebb tide (panels c and d). The left-hand column (a and c) shows the base run and the right-hand column (b and d) shows results from the future development model. The colour bar shows the horizontal depth-averaged current speeds ( $m.s^{-1}$ ).	19
Figure 17. Water levels during neap tide for location closest to the port developments (#9) for modelling scenarios base run (black line) and pre-2016 bathymetry (red dot-dash line). High and low tide are enlarged to highlight deviations affecting the tidal range.	20
Figure 18. Water levels during spring tide for location closest to port developments (#9) for modelling scenarios base run (black line) and pre-2016 bathymetry (red dot-dash line). High and low tide are enlarged to highlight deviations affecting the tidal range.	20
Figure 19. Differences in flow speeds between base run and pre-2016 dredging bathymetry. Differences at times closest (<30 mins from) to peak flood (a) and peak ebb (b) during neap tides. The colour bar indicates the velocity difference in $m.s^{-1}$ , with positive values corresponding to a reduction in velocity.	21
Figure 20. Differences in flow speeds between base run and pre-2016 dredging bathymetry. Differences at times closest (<30 mins from) to peak flood (a) and peak ebb (b) during spring tides. The colour bar indicates the velocity difference in $m.s^{-1}$ , with positive values corresponding to a reduction in velocity.	21
Figure A1.1. Calibration plots of measured (black dashed line) and modelled (solid blue line) water levels, current speeds, U velocities (east) and V velocities (north) from site #2 (Figure 3).	23
Figure A1.2. Calibration plots of measured (black dashed line) and modelled (solid blue line) water levels, current speeds, U velocities (east) and V velocities (north) from site #3 (Figure 3).	24
Figure A1.3. Calibration plots of measured (black dashed line) and modelled (solid blue line) water levels, current speeds, U velocities (east) and V velocities (north) from site #4 (Figure 3).	25
Figure A1.4. Calibration plots of measured (black dashed line) and modelled (solid blue line) water levels, current speeds, U velocities (east) and V velocities (north) from site #5 (Figure 3).	26
Figure A1.5. Calibration plots of measured (black dashed line) and modelled (solid blue line) water levels, current speeds, U velocities (east) and V velocities (north) from site #6 (Figure 3).	27
Figure A1.6. Calibration plots of measured (black dashed line) and modelled (solid blue line) water levels, current speeds, U velocities (east) and V velocities (north) from site #7 (Figure 3).	28
Figure A1.7. Calibration plots of measured (black dashed line) and modelled (solid blue line) water levels, current speeds, U velocities (east) and V velocities (north) from site #8 (Figure 3).	29
Figure A1.8. Calibration plots of measured (black dashed line) and modelled (solid blue line) water levels, current speeds, U velocities (east) and V velocities (north) from site #9 (Figure 3).	30

## Table of Tables

Table 1. Instrument types and locations. Numbers increase southward and correspond to instrument locations shown in Figure 1. All instruments measured three components of velocity and pressure. ADCPs and ADPs record a vertical profile of velocities. ADVs record velocities at a single fixed point.	8
Table 2: Tidal constituents used to force the model at the open boundaries. Phases are given in GMT.	10
Table 3. Bottom roughness maps defining bottom roughness (Chézy) coefficients based on water depths were tested during the calibration process. This table summarises the values used for specific depth ranges.	10
Table 4: Performance statistics of model calibration for water levels: the root-mean-squared error (RMSE), mean absolute error (MAE) and Brier skill score (BSS). The classification in the right-hand column is based on the BSS scheme proposed by Sutherland <i>et al</i> (2004).	11
Table 5: Performance statistics of model calibration for flow speeds: the root-mean-squared error (RMSE), mean absolute error (MAE) and Brier skill score (BSS). The classification in the right-hand column is based on the BSS scheme proposed by Sutherland <i>et al</i> (2004).	12
Table 6: Performance statistics of model validation for water levels: the root-mean-squared error (RMSE), mean absolute error (MAE) and Brier skill score (BSS). The classification in the right-hand column is based on the BSS scheme proposed by Sutherland <i>et al</i> (2004).	13
Table 7: Performance statistics of model validation for flow speeds: the root-mean-squared error (RMSE), mean absolute error (MAE) and Brier skill score (BSS). The classification in the right-hand column is based on the BSS scheme proposed by Sutherland <i>et al</i> (2004).	14

## Executive Summary

The impact of the Stella Development Plan, specifically proposed wharf, reclamation and channel extensions, on the hydrodynamics of Tauranga Harbour were investigated using a depth-averaged barotropic numerical model, Delft3D. The model was calibrated and validated using field observations collected in March 2017 after the completion of capital dredging in 2016. The model calibration and validation scores for water level were consistently excellent. Calibration and validation scores for velocity were mostly excellent, but some locations outside the region of interest had lower scores; but are not considered to impact on the reported results.

Water elevation changes resulting from the proposed extensions were less than the calibration and validation errors, and indicate negligible impact on tidal elevation and timing. The main impact of the extensions was a large decrease in flow speed within the deepened channel in Stella Passage. No significant changes were evident beyond the extent of the channel extension, although there were some slight changes in flow direction associated with the abrupt depth transition into the new dredged channel.

Comparison between the harbour hydrodynamics before and after the 2015/2016 capital dredging indicated that previous studies that investigated potential impacts of port and marina developments adjacent to Stella Passage will still be valid beyond the immediate area of wharf and channel extension.

## Introduction

The Port of Tauranga Ltd have proposed extending the Mount Maunganui and Sulphur Point Wharves, reclaiming areas landwards of the new wharves, and extending the Stella Passage shipping channel (Figure 1). Approximately 5.9 ha of the Stella Passage extension is already consented (RC 62910), with an extra 8.5 ha proposed to provide access to the extended wharves. The effects of proposed extensions were previously examined by numerical modelling undertaken by McKenzie (2014) and Watson (2016).

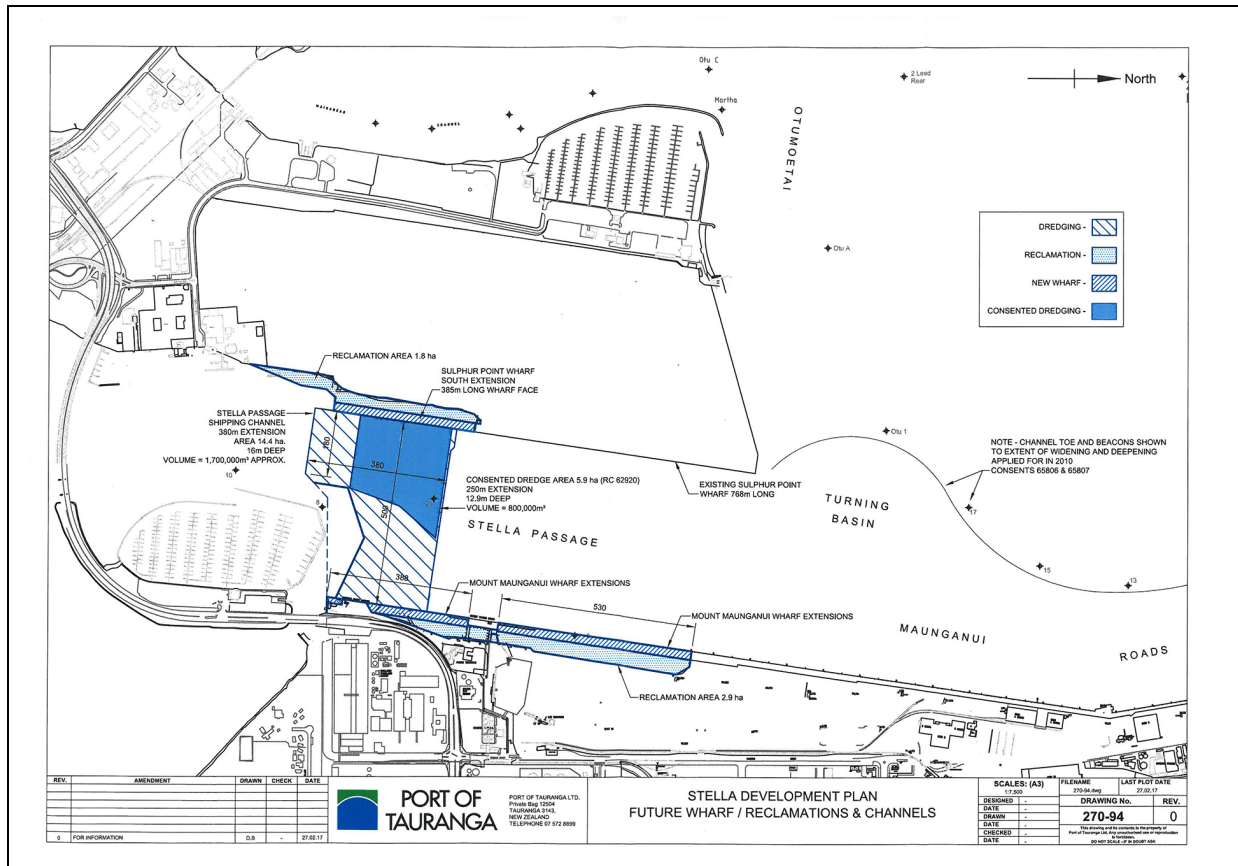


**Figure 1.** Proposed extensions to the Mount Maunganui and Sulphur Point Wharves, and Stella Passage shipping channel under the Port of Tauranga Ltd Stella Development Plan.

McKenzie (2014) focussed on the interactions between the consented dredging area and proposed breakwater developments for the Tauranga Bridge Marina, and considered the impacts on Waipu Bay, Town Reach and Stella Passage (Figure 2). Watson (2016) assessed the impacts of the Stella Development Plan (Figure 1) on the upper harbour, Town Reach and Stella Passage (Figure 2). Both studies used numerical models calibrated with pre-capital dredging bathymetry and field observations.

Boulay (2012) assessed the impacts of previous port developments on the seabed characteristics and benthic macrofauna of Town Reach and Stella Passage. He also produced detailed digital maps of the existing seabed and shellfish distributions to allow the effects of the 2015/2016 capital dredging and proposed marina developments to be assessed.

Brunschwiler (2015) undertook a series of field deployments within Stella Passage and the Maunganui Roads (Figure 2A) to monitor freshwater plumes due to stormwater discharge from outfalls beneath the Mount Maunganui Wharves. This included measurements of water elevations, currents, and water characteristics (suspended sediment, conductivity and temperature). Her data indicate that flows within Stella Passage and the junction with the

Otumoetai Channel and Maunganui Roads are modified by weather conditions and the influx of freshwater from stormwater drains.



**Figure 2.** Locations within the southeastern basin of Tauranga Harbour: (A) main components of the tidal inlet system (ETD and FTD are the ebb tidal delta and flood tidal delta respectively); and (B) main components of Stella Passage and the upper harbour. From Figures 2.2 & 2.3 of Watson (2016).

The purpose of this report is to repeat the previous modelling of Watson (2016) using the current (2017-2018) bathymetry and calibrated with measurements collected after the

completion of the capital dredging. In particular, the model will be compared to the earlier model to determine if the earlier impact assessments are still valid.

## Field observations



**Figure 3.** Google Earth image showing locations of instruments deployed during the field experiment undertaken in March and April 2017. Circles indicate Acoustic Doppler (Current) Profilers (ADCPs) and squares show Acoustic Doppler Velocimeters (ADVs)

A field experiment was undertaken in March and April 2017 to provide observational data of flow behaviour for model calibration following the 2015/2016 capital dredging. The instrument array was concentrated in and around the focus area for this study: the Port of Tauranga and Stella Passage (Figure 3). Details of instrumentation and sampling parameters are given in Table 1. A further deployment was undertaken in April 2018 to assess the impacts of the capital dredging for areas south of the Railway Bridge (site 9 in Figure 3). These data were not used for model calibration, but will be used to verify model results from this and previous studies in a separate report.

Pressure data were corrected for atmospheric variations using hourly pressure data obtained from the Thames Automatic Weather Station, which is highly correlated with the University of Waikato weather station on the Omokoroa Peninsula and the Port of Tauranga weather

station at Tug Berth, and provides a longer and more complete time series of observations than other available stations. Data from above the water surface, and from 1 or 2 depth bins below the water surface, were removed to avoid side-lobe acoustic interference, and then averaged over the depth of the profile. Velocities were rotated to an ENU (East-North-Up) coordinate system.

**Table 1.** Instrument types and locations. Numbers increase southward and correspond to instrument locations shown in Figure 1. All instruments measured three components of velocity and pressure. ADCPs and ADPs record a vertical profile of velocities. ADVs record velocities at a single fixed point.

Number	Type	Make	Model	Cell size (m)	Time averaging window (min)	Profile interval (min)
1	ADCP	Nortek	Aquadopp	1	3	10
2	ADV	Nortek	Vector	-	54 s	10
3	ADV	Sontek	Triton	-	6	10
4	ADCP	Nortek	Aquadopp	0.5	8	10
5	ADV	Sontek	Triton	-	6	10
6	ADP	Sontek	Argonaut	0.5	7	10
7	ADV	Nortek	Vector	-	54 s	10
8	ADCP	Nortek	Aquadopp	0.5	3	10
9	ADV	Sontek	Triton	-	6	10

## Numerical modelling

Numerical modelling was undertaken using the hydrodynamic package Delft3D in depth-averaged barotropic mode (2D). This open-source software solves the unsteady shallow water equations for an incompressible fluid and has been extensively validated (e.g. Elias et al., 2000; Lesser et al., 2004). A domain decomposed grid was implemented with a resolution of 40 m in the inner southern harbour, 20 m inside and south of Stella Passage and 80 m offshore (Figure 4).

The model was similar to a previously calibrated model by Watson (2016); however, the present model incorporates new multibeam bathymetric data provided by the Port of Tauranga following dredging of shipping channels in 2015/2016. Bathymetry in other areas was generated by combining high-resolution LiDAR scans from the Bay of Plenty Regional Council (BoPRC), the Port of Tauranga and Land Information New Zealand (LINZ) bathymetry data (all referenced to Mean Level of the Sea datum) (Figure 5).

The model was forced by 8 tidal constituents (Table 2) extracted from 1999 water level data obtained from the Moturiki Island wave buoy to be consistent with previous models used to assess the impacts of port development (see Watson, 2016). No wind or wave forcing or freshwater input was applied. The model was run for a 33 day period spanning the field deployments. The initial three days of the simulations were discarded to allow for model spin-up. The time step was 15 s, which satisfies the Courant condition. Observation points were added within the model to correspond to the locations of field instruments from the March 2017 and previous deployments in Tauranga Harbour.

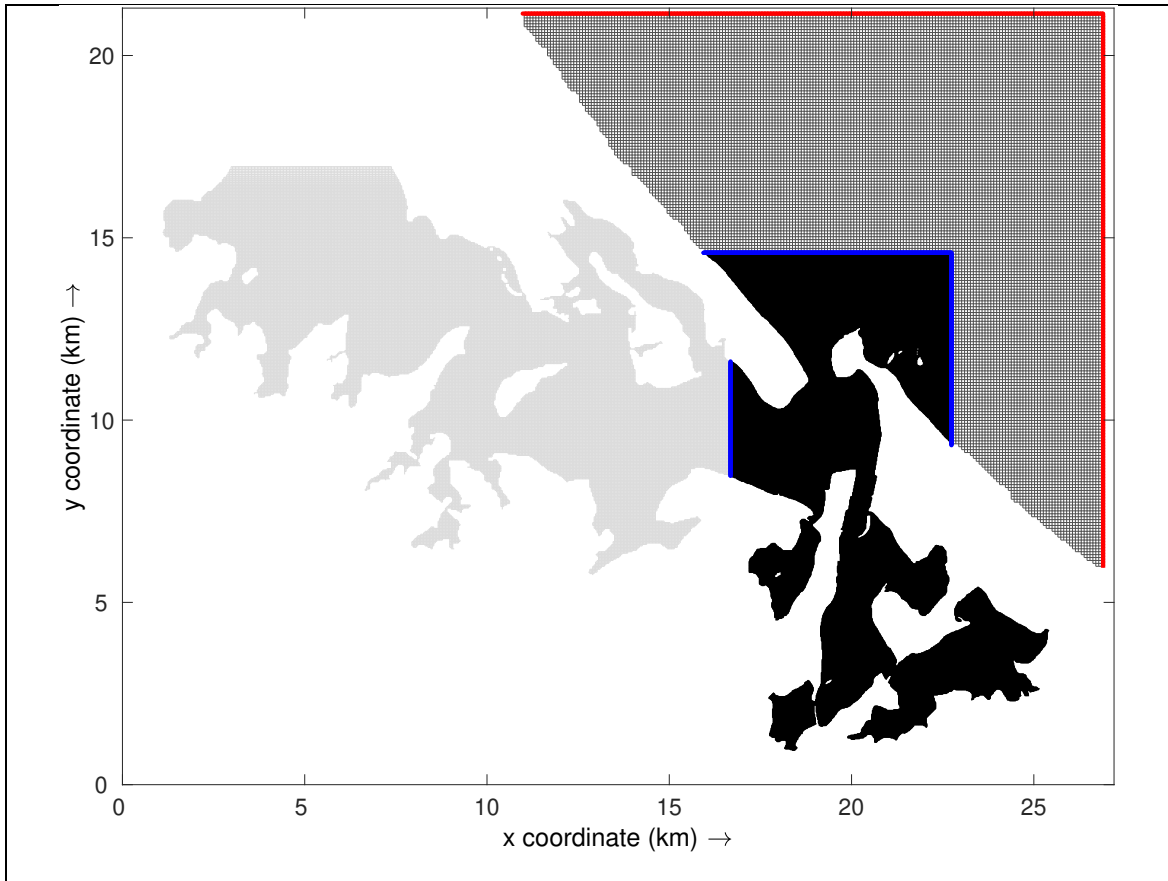


**Figure 4.** Numerical grid of the southern Tauranga Harbour. Grid resolution was 40, 20 and 80 m in the light grey, black, and dark grey domains, respectively. Domain decomposition boundaries between grids are shown in blue. Open boundaries at which forcing is applied are shown in red.

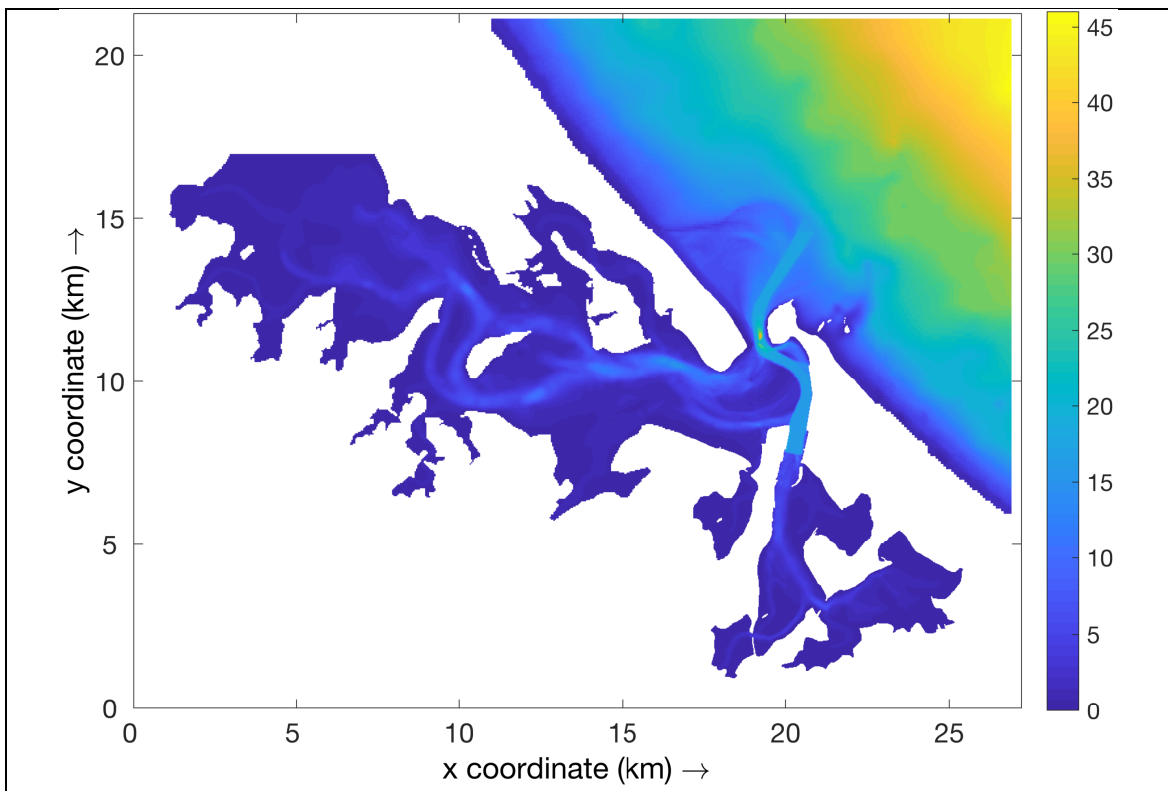


**Figure 5:** Model bathymetry. The colour bar on the right shows depth in metres.

**Table 2:** Tidal constituents used to force the model at the open boundaries. Phases are given in GMT.

Tidal constituent	Amplitude (m)	Phase ( $^{\circ}$ GMT)
M2	0.748	189.70
S2	0.098	262.99
N2	0.167	154.42
K2	0.019	266.91
K1	0.051	180.74
P1	0.016	174.87
Q1	0.002	50.19
O1	0.011	126.71

## Model calibration

The model was calibrated against field data by varying eddy viscosity and bottom friction. Bottom friction was found to have the strongest influence out of parameters investigated in a sensitivity analysis for Tauranga Harbour by Watson (2016), and eddy viscosity influences the formation of eddies that are known to exist within Stella Passage. A uniform bottom friction coefficient and four spatially varying bottom friction (bed roughness) maps were evaluated (Table 3). Once a bottom roughness map was selected, simulations using four different eddy viscosities (6, 8, 10 and 12  $\text{m}^2/\text{s}$ ) were conducted. Model performance was assessed over a 7-day calibration period corresponding to the beginning of the field deployment (Figure 6). The calibrated model was then chosen based on a compromise between good performance metrics in the key areas of interest (Town Reach and Stella Passage, and the Railway Bridge at site #9), whilst still retaining overall model performance in other areas (sites within the harbour #2 to #8, Figure 3).

**Table 3.** Bottom roughness maps defining bottom roughness (Chézy) coefficients based on water depths were tested during the calibration process. This table summarises the values used for specific depth ranges.

Chézy Value ( $\text{m}^{1/2} \text{s}^{-1}$ )	Elevation Range (m MSL)				
	Option 1	Option 2	Option 3	Option 4	Option 5
65	all depths	-	-	<-5	<-7
55		<-5	<-2	-5 to -2	-7 to -3
45		-5 to -2	-2 to -1	-2 to -1	-3 to -1.5
35		-2 to 0.5	-1 to 1.5	-1 to 1.5	-1.5 to 1.5
7		0.5 to 5	1.5 to 7	1.5 to 7	1.5 to 7
1		>5	>7	>7	>7

Model calibration results from all 8 sites within the harbour (Figure 3) are shown in Appendix One. In general, the model predicted water levels and velocity magnitudes well, although it did not always reproduce the velocities in the less dominant flow direction. Standard model performance statistics are given in Tables 4 and 5, consisting of the: root-mean-squared error (RMSE), mean absolute error (MAE) and Brier skill score (BSS). The overall model skill was evaluated using the classification scheme of Sutherland (2004) based

on the Brier Skill Score (using the mean of the observational data over the calibration period as the baseline).

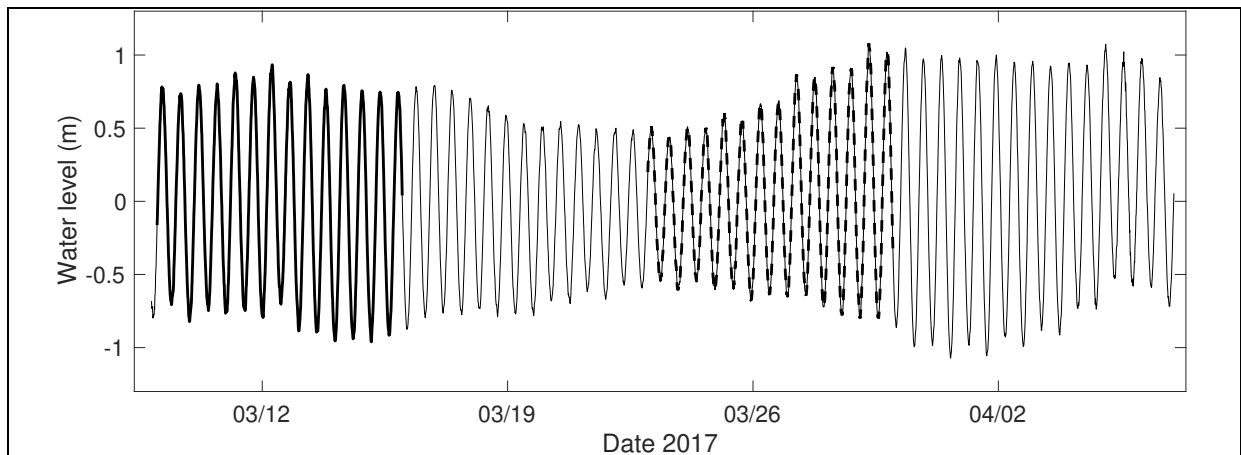


**Figure 6.** Pressure time series from site #1 (outside the harbour). Sections of the time series used for calibration and validation are shown in thick solid and thick dashed lines, respectively.

The water level predictions were classified as “excellent” at all sites (Table 4), while velocities were “excellent” at 5 sites, “good” at site 9 and “bad” at sites 4 and 7 (Table 5). At site 4, models overpredicted flow speeds by up to ~30%. However, site 4 is located in an area subjected to highly variable eddies associated with the flood jet, which are not considered likely to be impacted by flow changes in Stella Passage. Hence, a “bad” classification for this site is not of concern.

**Table 4:** Performance statistics of model calibration for water levels: the root-mean-squared error (RMSE), mean absolute error (MAE) and Brier skill score (BSS). The classification in the right-hand column is based on the BSS scheme proposed by Sutherland et al (2004).

Site	MAE (m)	RMSE (m)	BSS	Classification (Sutherland et al., 2004)
2	0.0782	0.0993	0.9677	Excellent
3	0.1108	0.1381	0.9369	Excellent
4	0.0919	0.1191	0.9523	Excellent
5	0.1033	0.1323	0.9315	Excellent
6	0.1067	0.1336	0.9275	Excellent
7	0.076	0.0935	0.9721	Excellent
8	0.0735	0.0901	0.9746	Excellent
9	0.0953	0.1202	0.9473	Excellent

Site 7 is located near the junction of the Maunganui Roads, Otumoetai Channel and Stella Passage. Due to vessel movements, it was necessary to place the instrument close to a channel marker on the edge of Centre Bank. This site is not an ideal location to measure flows, and the observational data had some data gaps (likely owing to algae on the sensor), which may have contributed to overall poor performance. Previous modelling has also had difficulty obtaining a good calibration for this location (Bell, 1991; Watson, 2016), and field observations by Brunschwiler (2015) indicate that the flows at this location are influenced by wind conditions. Site 7 is not assessed as an area of concern in relation to potential impacts by the southern expansion, as the excavation of a turning basin provided for by existing consents will have a larger impact than the development considered by this modelling. Therefore, the “bad” classification is considered acceptable.

**Table 5:** Performance statistics of model calibration for flow speeds: the root-mean-squared error (RMSE), mean absolute error (MAE) and Brier skill score (BSS). The classification in the right-hand column is based on the BSS scheme proposed by Sutherland *et al* (2004).

Site	MAE (m)	RMSE (m)	BSS	Classification (Sutherland et al., 2004)
2	0.0844	0.0988	0.5385	Excellent
3	0.1368	0.1904	0.6903	Excellent
4	0.2448	0.2855	-0.1861	Bad
5	0.0802	0.1051	0.8119	Excellent
6	0.0516	0.0639	0.7377	Excellent
7	0.133	0.1601	-2.5048	Bad
8	0.0852	0.1121	0.675	Excellent
9	0.1046	0.1309	0.2763	Good

The final calibrated model used the spatially varying bed roughness map specified by option 5 (Table 3 and shown in Figure 7) and an eddy viscosity of  $12 \text{ m}^2/\text{s}$ .

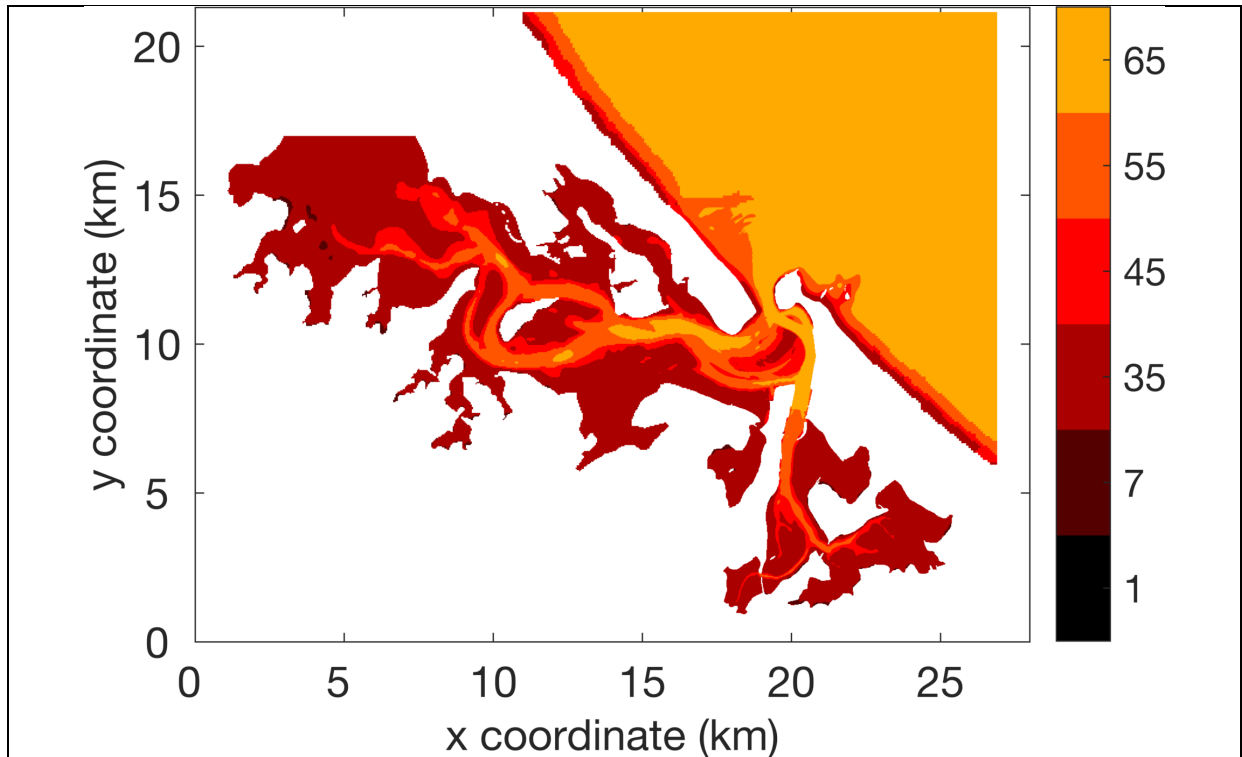


**Figure 7:** Spatially varying bottom roughness map used in calibrated model. The colour bar shows the Chézy coefficient ( $\text{m}^{1/2} \text{ s}^{-1}$ ).

Differences between model predictions and observations can arise due to a number of factors. The model bathymetry was based on a number of sources including LINZ charts and resolution of the bathymetric data varied. Interpolation across multiple-resolutions combined with the necessity of discretising a continuous real world system may have contributed to some of the errors, particularly in regions with rapidly varying topography at the edge of channels (as is the case with site #4). Winds and wave forcing was neglected in the model; however, previous models have indicated these effects are generally small (McKenzie, 2014),

although measurements reported by Brunschwiler (2015) indicate that flows in some locations (eg. Site #7) respond to wind and rainfall. Hence, any potential improvement does not justify the increased computational time for their inclusion in the present model. Freshwater forcing was also not included in the present model as in the key area of interest, average flow inputs are small (1-3 m<sup>3</sup>/s) justifying their neglect. Other differences between predictions and observations may have arisen due to errors in the measurements themselves: Small changes in instrument directions can contribute to slight changes in velocity components. Moreover, some instruments recorded single point measurements close (~1 m) to the bed. While the harbour is generally well-mixed, small differences between near bed and depth-averaged measurements would contribute to part of the discrepancies between model and observations, with the model appearing to “over-predict” flow speeds (such as at Site #7).

## Validation results

Model performance was also validated against a 7-day period from 23 March to 30 March 2017 capturing a neap to spring transition (Figure 6). Model performance statistics for the validation period are given in Tables 6 and 7.

**Table 6:** Performance statistics of model validation for water levels: the root-mean-squared error (RMSE), mean absolute error (MAE) and Brier skill score (BSS). The classification in the right-hand column is based on the BSS scheme proposed by Sutherland *et al* (2004).

Site	MAE (m)	RMSE (m)	BSS	Classification (Sutherland et al., 2004)
2	0.0549	0.0715	0.9779	Excellent
3	0.059	0.0743	0.9758	Excellent
4	0.0654	0.078	0.9732	Excellent
5	0.067	0.085	0.9625	Excellent
6	0.0823	0.1038	0.9403	Excellent
7	0.0543	0.0698	0.9795	Excellent
8	0.0541	0.067	0.9817	Excellent
9	0.0638	0.0775	0.9725	Excellent

The validation for water level was classified as “Excellent” at all sites. Similarly, velocities were classified as “excellent” or “good” for all sites, except site 7 at which data coverage was relatively sparse and there are difficulties with the location as discussed above. Thus, it was concluded there was sufficient confidence in model predictions to examine key areas of interest.

**Table 7:** Performance statistics of model validation for flow speeds: the root-mean-squared error (RMSE), mean absolute error (MAE) and Brier skill score (BSS). The classification in the right-hand column is based on the BSS scheme proposed by Sutherland *et al* (2004).

Site	MAE (m)	RMSE (m)	BSS	Classification (Sutherland et al., 2004)
2	0.0626	0.0778	0.6988	Excellent
3	0.1509	0.1929	0.6538	Excellent
4	0.1726	0.2114	0.2999	Good
5	0.0897	0.1181	0.7509	Excellent
6	0.0802	0.1943	0.2839	Good
7	0.1158	0.1838	-0.2563	Bad
8	0.0729	0.093	0.6871	Excellent
9	0.076	0.1057	0.5148	Excellent

## Model scenarios

Results from the calibrated model (hereafter referred to as the “base run”) were compared to those from two different modelling scenarios (Figure 8):

- Future development model. A model was set up to include proposed changes to the Port of Tauranga under the Stella Development Plan, namely dredging of the southern end of Stella Passage to 16 m water depth, and land reclamations and wharf extensions (Figure 1).
- Pre-2016 dredging. This model will be used to assess the quality of the previous modelling predictions (relative to the present-day bathymetry).

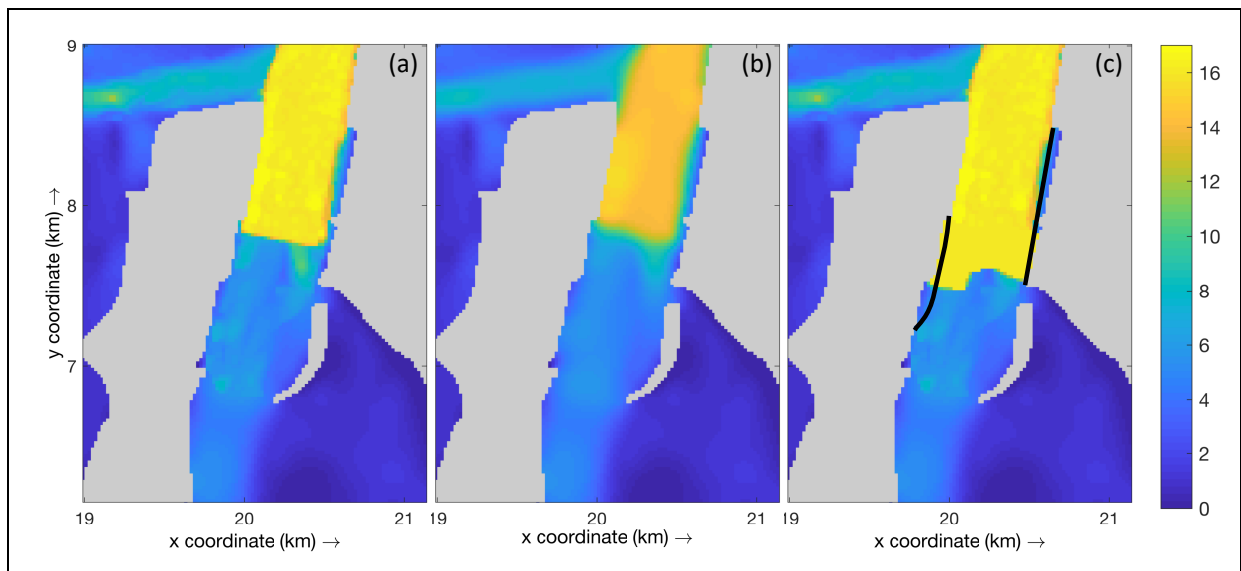


**Figure 8.** Bathymetries for all modelled scenarios for development of the Port of Tauranga. The colour bar shows depth in m: (a) Base run; (b) pre-2016 dredging; and (c) future development model. In (c), the black lines show the approximate location of the thin dams representing land reclamation and wharf extensions.

For both scenarios, a spatially varying roughness map based on option 5 (Table 3) was applied. All other forcing remained the same as the base run. The wharf reclamations and

land reclamations were represented in the model as “thin dams”. These stop all flow across the grid cell boundary (rather than just reducing flow as would occur with the addition of wharf pylons) and hence represent the largest possible impact of the wharf construction.

The bathymetry maps used in the base run and scenarios are shown in Figure 8. The precise grid locations of the thin dams in Figure 8c are shown in Figure 9.

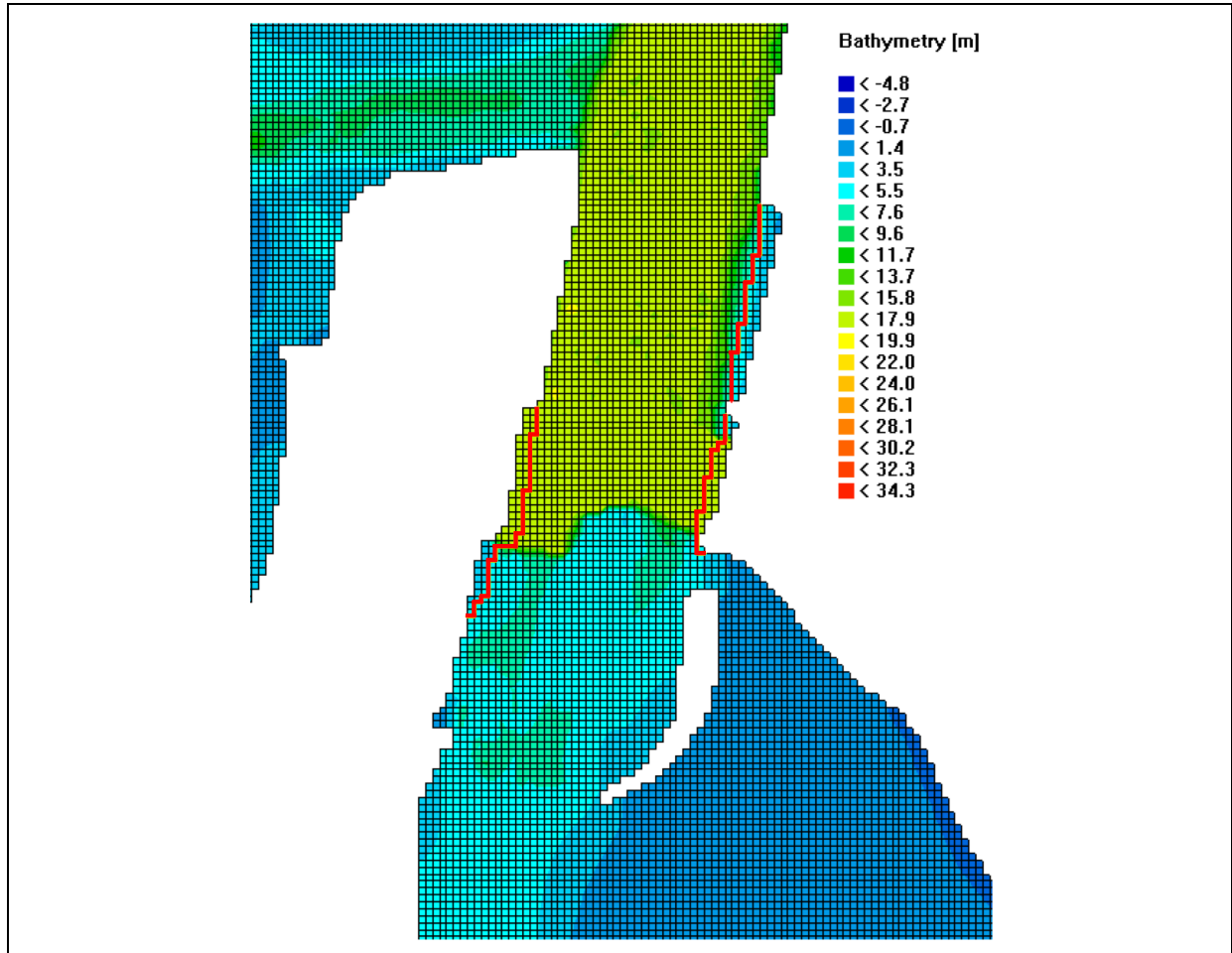


**Figure 9.** Precise grid locations of thin dams (thick red lines) used in the future development model to represent land reclamation and wharf extensions.

### Results from scenario simulations: Comparison between the base run (present conditions) and future development model

Modelled water levels at the observation site closest to the dredging (site #9) are shown for a neap (Figure 10). No clear difference can be discerned: for the time period shown in the figure, the maximum and mean difference between modelled water levels were 2.1 and 1.1 mm, respectively. Similarly, differences in water levels between the modelled scenarios during spring tide (Figure 11), while larger than for neap conditions, were still very small (maximum 5.5 mm and mean 2.5 mm). These values are smaller than the calibration errors (Table 4) and similar to or smaller than the validation errors (Table 6). Therefore, these differences are negligible.

Figures 12 and 13 show differences in current speeds between the two scenarios for a neap and spring tide, respectively. Panels show the output timesteps closest to the expected peak flood (~25 minute before) and peak ebb (~5 minute before) velocities. The figures clearly demonstrate that changes from planned port developments are highly localised to the dredged area (Figure 1), and (unsurprisingly) greater on spring than neap tides. Additionally, the

spatial extent of the difference is slightly larger during ebb than flood tides as the system is ebb dominant at this location (ebb velocities greater than flood velocities).

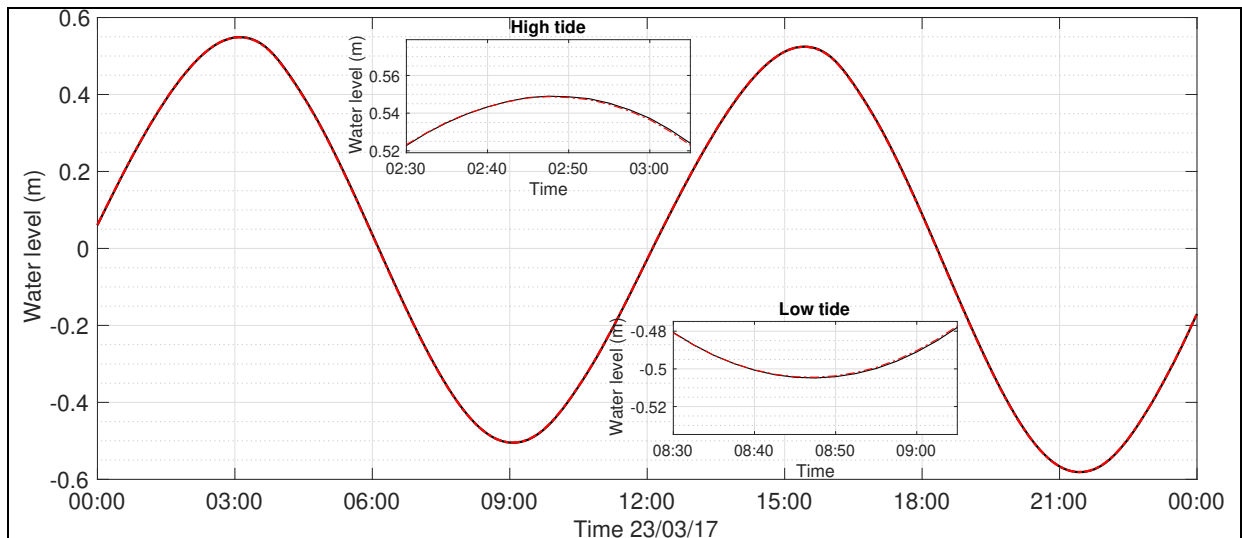


**Figure 10.** Water levels during neap tide for location closest to port developments (#9) for modelling scenarios base run (black line) and future development model (red dot-dash line). High and low tide are enlarged to highlight deviations affecting the tidal range.

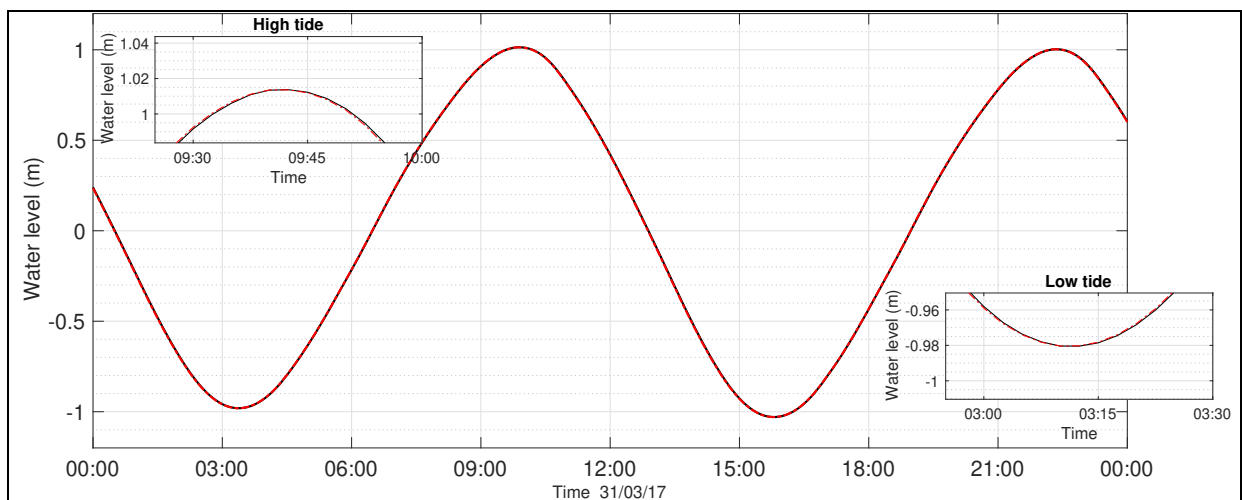


**Figure 11.** Water levels during spring tide for location closest to port developments (#9) for modelling scenarios base run (black line) and future development model (red dot-dash line). High and low tide are enlarged to highlight deviations affecting the tidal range.

Figure 14 shows a close up of the areas adjacent to the proposed port developments. Large velocities differences behind wharf additions and land reclamations (represented by thin dams) occur as all flow is prevented by the thin dams. Positive differences (indicating reduced velocities) of up to  $0.5 \text{ m.s}^{-1}$  occur directly over the dredged regions. These slower flow velocities are expected from mass conservation (i.e. the same amount of water pushed through larger cross-sectional area); however, the large changes ( $0.3$  to  $0.5 \text{ m.s}^{-1}$ ) are confined to within  $40 \text{ m}$  of dredged area, while smaller changes ( $<0.05 \text{ m.s}^{-1}$ ) are visible up to  $\sim 250 \text{ m}$  from dredged region.

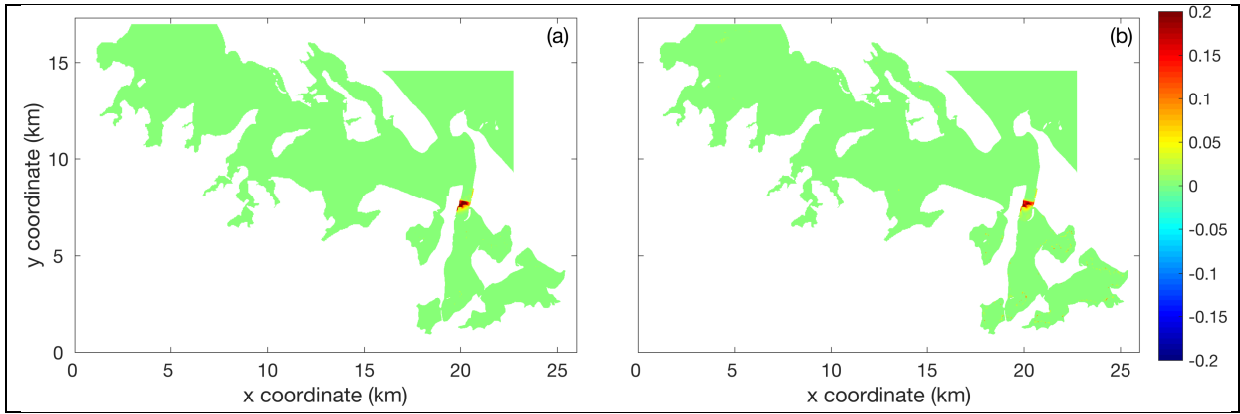


**Figure 12.** Differences in flow speeds in  $m.s^{-1}$  between base run and future development model. Differences at times closest (<30 mins from) to peak flood (a) and peak ebb (b) during neap tides. The colour bar indicates the velocity difference in  $m.s^{-1}$ , with positive values corresponding to a reduction in velocity.

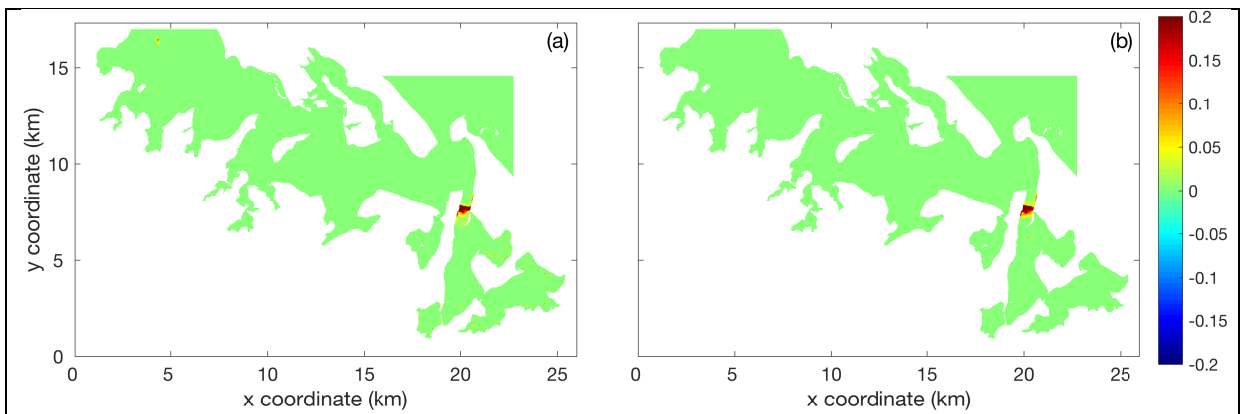


**Figure 13.** Differences in flow speeds in  $m.s^{-1}$  between base run and future development model. Differences at times closest (<30 mins from) to peak flood (a) and peak ebb (b) during spring tides. The colour bar indicates the velocity difference in  $m.s^{-1}$ , with positive values corresponding to a reduction in velocity.

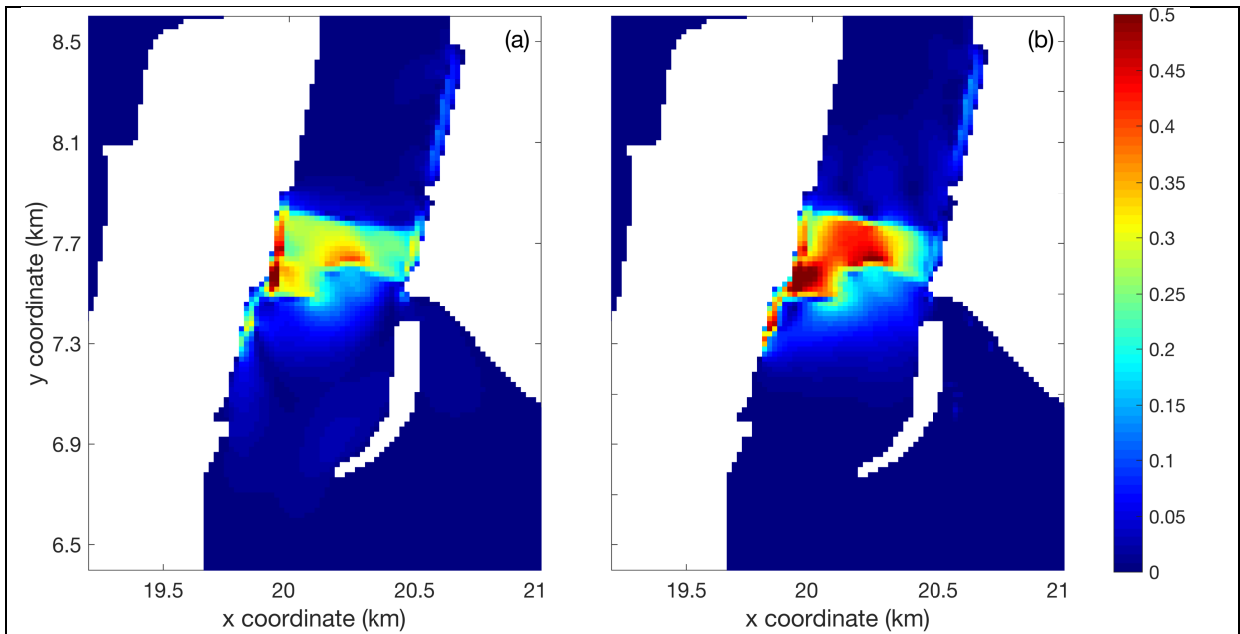


**Figure 14.** Close up showing predicted differences in flow speeds in  $m.s^{-1}$  between base run and future development model in area around the Port of Tauranga. Differences at times closest (<30 mins from) to peak flood (a) and peak ebb (b) during spring tides. The colour bar indicates the velocity difference in  $m.s^{-1}$ , with positive values corresponding to a reduction in velocity.

Figure 14 indicates that no significant flow increase is predicted between the dredged area and the Harbour Bridge, or the channel into Waipu Bay. However, there are minor changes in flow orientations as indicated by a comparison of the velocity vectors shown in Figures 15 and 16. Only small differences between the base run and future development models are visible: at the southern end of Stella Passage, the across-channel flow is less uniform in the future development scenario owing to a slight flow reduction around (20, 7.5).

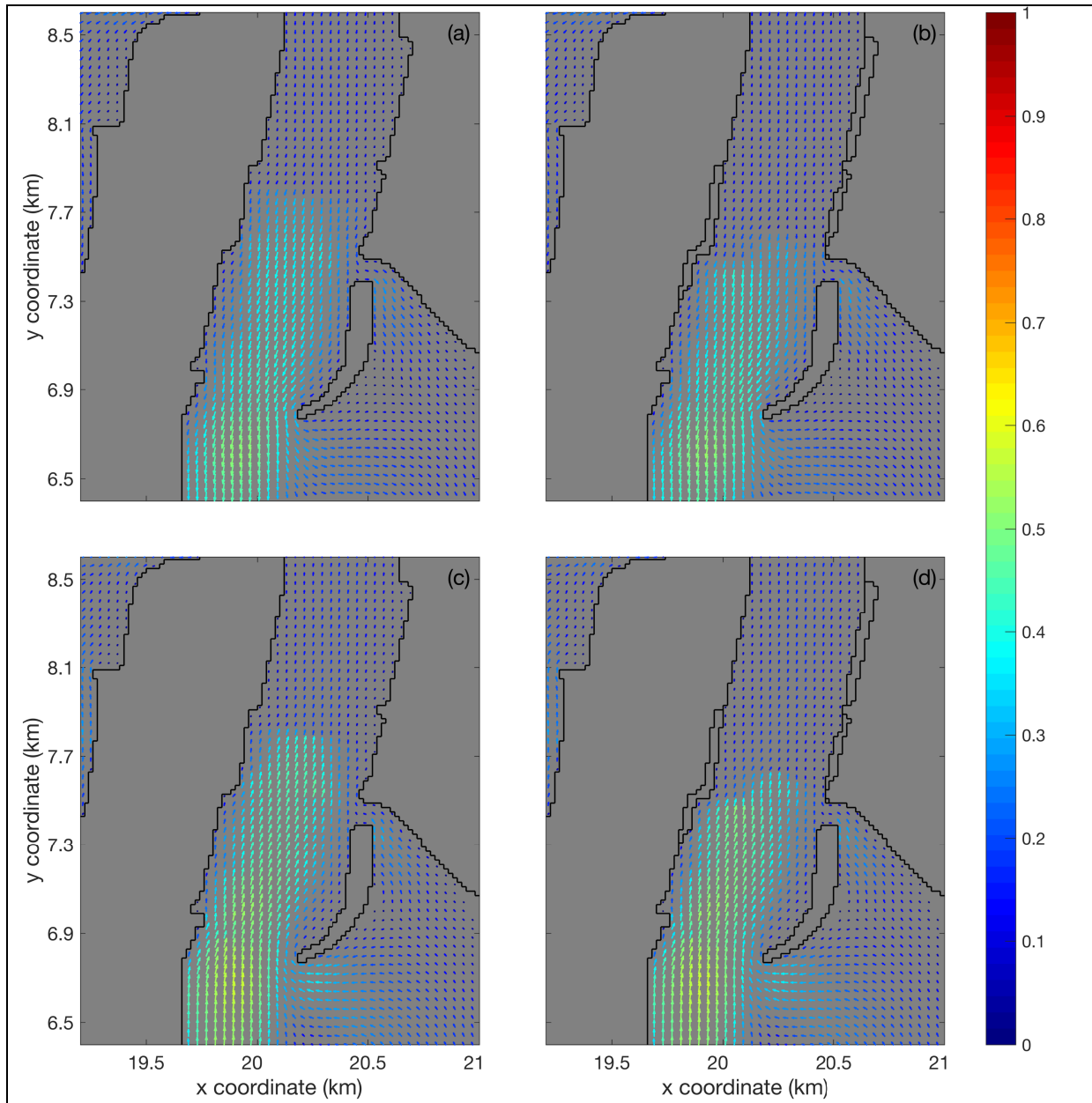


**Figure 15.** Velocity vectors during neap tides in the area of proposed port developments. Results from times closest (<30 mins from) to peak flood tide (a and b) and peak ebb tide (panels c and d). The left-hand column (a and c) shows the base run and the right-hand column (b and d) shows results from the future development model. The colour bar shows the horizontal depth-averaged current speeds ( $\text{m.s}^{-1}$ ).

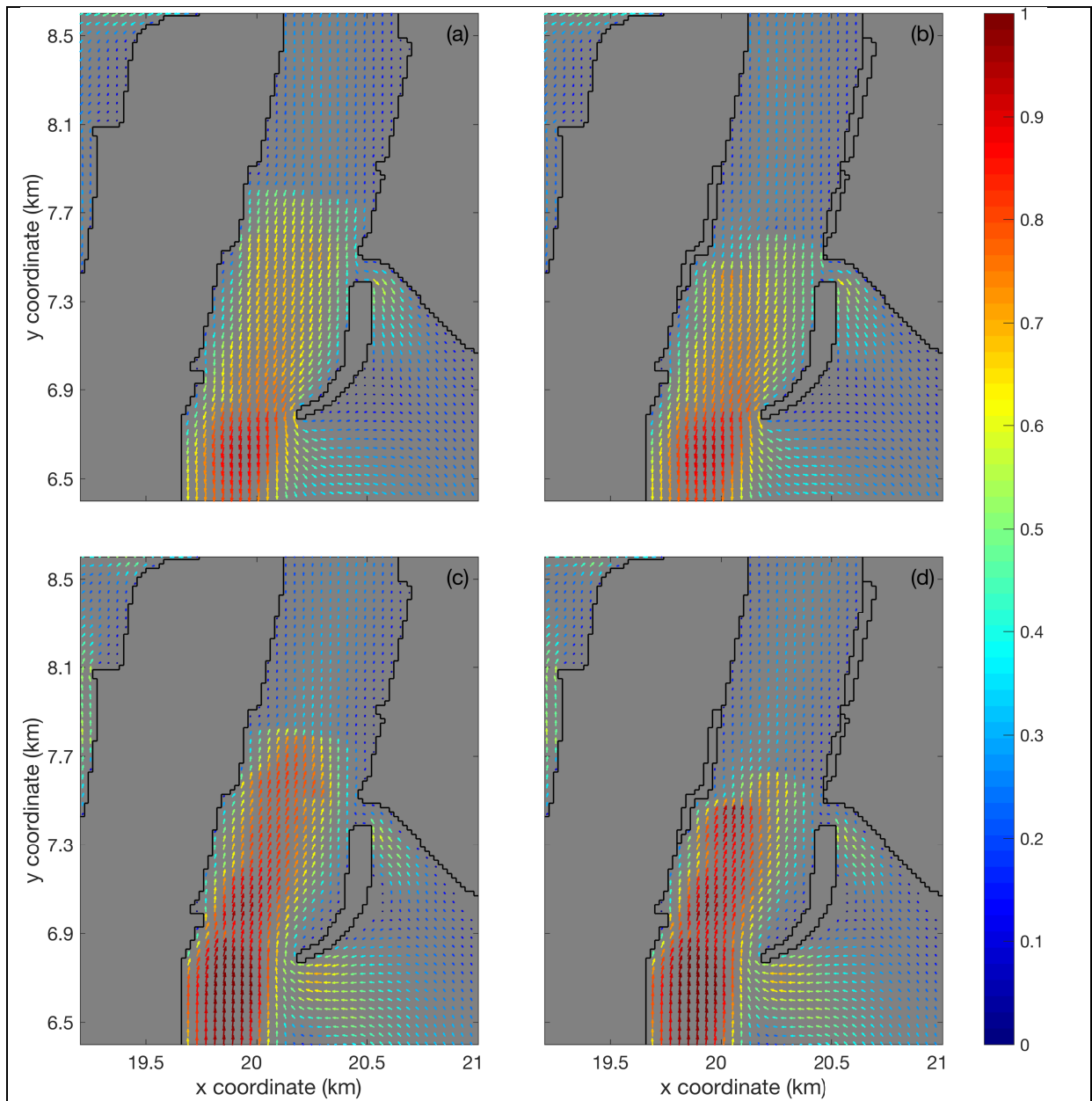


**Figure 16.** Velocity vectors during spring tides in the area of proposed port developments. Results from times closest (<30 mins from) to peak flood tide (a and b) and peak ebb tide (panels c and d). The left-hand column (a and c) shows the base run and the right-hand column (b and d) shows results from the future development model. The colour bar shows the horizontal depth-averaged current speeds ( $\text{m}\cdot\text{s}^{-1}$ ).

### Results from scenario simulations: Comparison between present (base run) and former (pre-2016 dredging) bathymetries.

To assess the magnitude of the proposed extensions relative to the impacts of the 2015-2016 capital dredging, the base and pre-2016 bathymetry models were compared. Predictions of water levels at site 9, show very small changes albeit larger than those discussed above (Figures 10 & 11). Maximum and mean differences in water levels were 0.017 m and 0.009 m, respectively, during neap tides (Figure 17), and 0.05 and 0.023 m during spring tides (Figure 18). These differences were partially due to a delay of around 6 to 10 minutes in the propagation of the tidal wave (ie. phase shifts) and a small reduction in tidal amplitude. The changes exceed the calibration and validation errors.

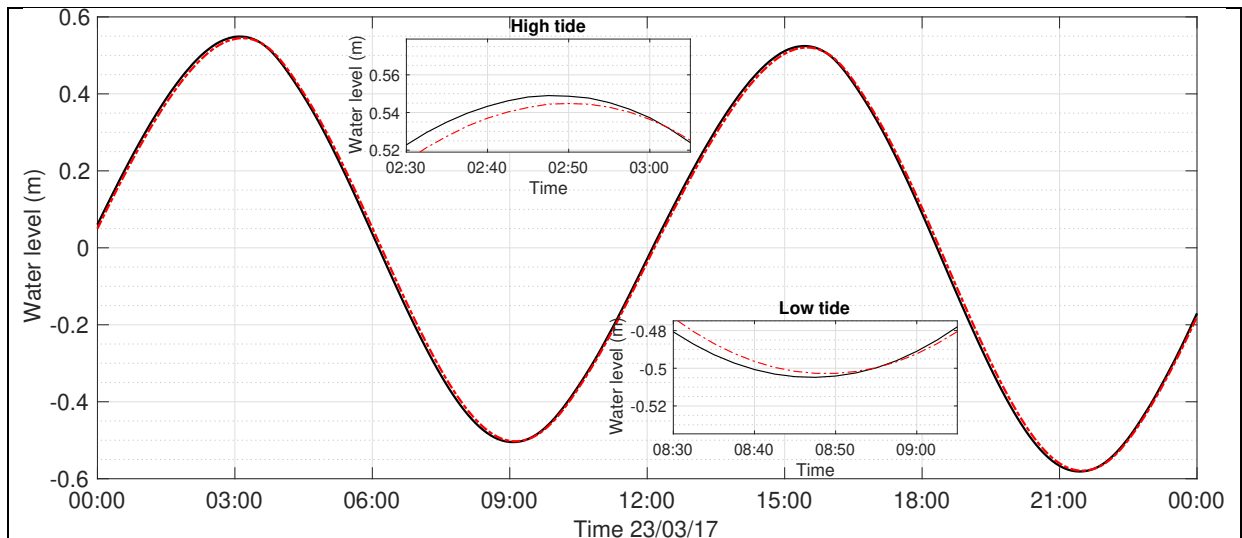


**Figure 17.** Water levels during neap tide for location closest to the port developments (#9) for modelling scenarios base run (black line) and pre-2016 bathymetry (red dot-dash line). High and low tide are enlarged to highlight deviations affecting the tidal range.

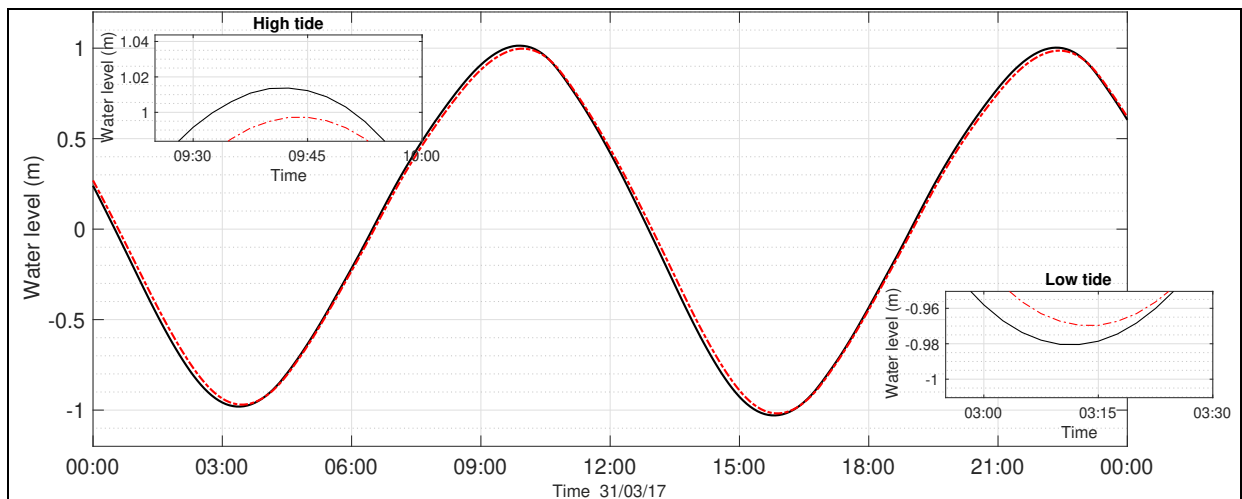


**Figure 18.** Water levels during spring tide for location closest to port developments (#9) for modelling scenarios base run (black line) and pre-2016 bathymetry (red dot-dash line). High and low tide are enlarged to highlight deviations affecting the tidal range.

Differences in flow speeds between the base and pre-2016 dredging models were  $<0.4 \text{ m.s}^{-1}$  and mostly consisted of speed reductions confined to the vicinity of the dredged regions (Figures 19 and 20). The largest changes occurred around the Harbour Entrance, including Cutter Channel, Lower Western Channel and the flood ramp on Centre Bank. The southern end of the dredged channel in Stella Passage also showed a significant reduction in flow speed.

## Conclusions

The modelled Stella Development Plan wharf and channel extensions showed no significant changes to water elevations and depth-averaged current velocities beyond the immediate vicinity of the extensions. These results indicate that the previous modelling by McKenzie (2014) for Waipu Bay, and Watson (2016) for the upper southern Tauranga Harbour is still valid even without incorporating the current bathymetry for the shipping channels.

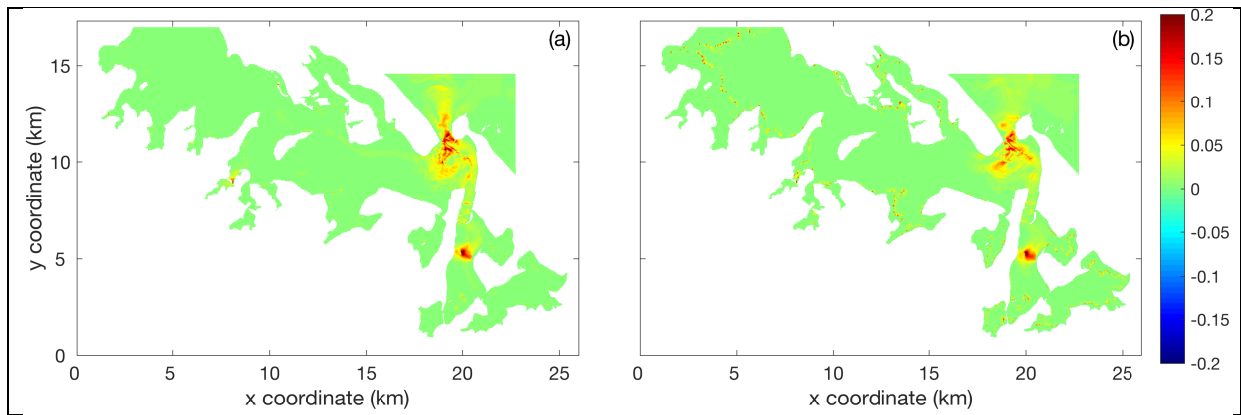


**Figure 19.** Differences in flow speeds between base run and pre-2016 dredging bathymetry. Differences at times closest (<30 mins from) to peak flood (a) and peak ebb (b) during neap tides. The colour bar indicates the velocity difference in  $\text{m.s}^{-1}$ , with positive values corresponding to a reduction in velocity.

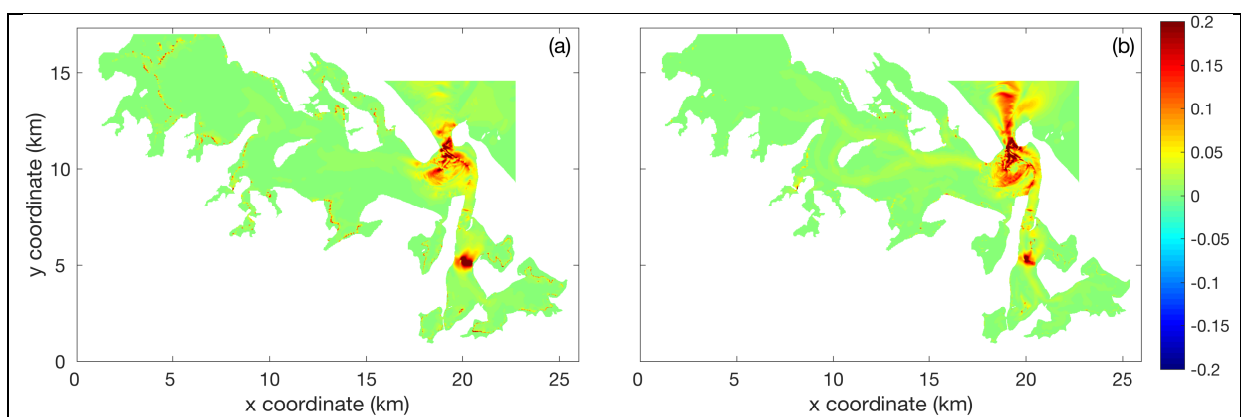


**Figure 20.** Differences in flow speeds between base run and pre-2016 dredging bathymetry. Differences at times closest (<30 mins from) to peak flood (a) and peak ebb (b) during spring tides. The colour bar indicates the velocity difference in  $\text{m.s}^{-1}$ , with positive values corresponding to a reduction in velocity.

Overall, the larger increase in channel volume associated with the 2015-2016 capital dredging had a larger impact on the hydrodynamics within the port area than the proposed extensions. Further, the modelling indicates no impact beyond the immediate vicinity of the dredging for the capital dredging, confirming the restricted impact predicted for the much smaller proposed extensions.

## References

- Bell, R.G. (1991), Port of Tauranga Model Study (Deepened shipping channel proposal), Consultancy Report No 6127/1 prepared for Port of Tauranga Ltd, Water Quality Centre, DSIR, Hamilton, 22 pp.
- Boulay, S.O.C. (2012). Analysis of multibeam sonar data for benthic habitat characterization of the Port of Tauranga, New Zealand, MSc thesis, University of Waikato, Hamilton, New Zealand.
- Brunschwiler, N.R. (2015). Dispersal and mixing of stormwater run-off plumes in the Port of Tauranga, New Zealand, MSc thesis, University of Waikato, Hamilton, New Zealand
- Deltares (2017). Delft3D-FLOW User Manual, version 3.15.49946. Deltares.
- Elias, E., D. Walstra, J. Roelvink, M. Stive, and M. Klein (2000), Hydrodynamic validation of Delft3D with field measurements at Egmond, *Coastal Engineering*, pp. 2714–2727, Am. Soc. of Civ. Eng., Sydney, Australia.
- Lesser, G. R., J. A. Roelvink, J. van Kester, and G. S. Stelling (2004), Development and validation of a three-dimensional morphological model, *Coastal Engineering*, 51(8–9), 883–915.
- McKenzie, J. S. (2014). Predicted hydrodynamic and sediment transport impacts of breakwater construction in Tauranga Harbour, New Zealand. M.Sc. thesis, University of Waikato, Hamilton, New Zealand.
- Sutherland, J., A.H. Peet, and R.L. Soulsby (2004), Evaluating the performance of morphological models. *Coastal Engineering*, 51(8–9), pp. 917-939.

Watson, H.M. (2016). Potential impacts of wharf extensions on the hydrodynamics of Stella passage and upstream regions of Tauranga Harbour, New Zealand. M.Sc thesis, University of Waikato, Hamilton, New Zealand.

## Appendix One – Calibration plots (PUV)

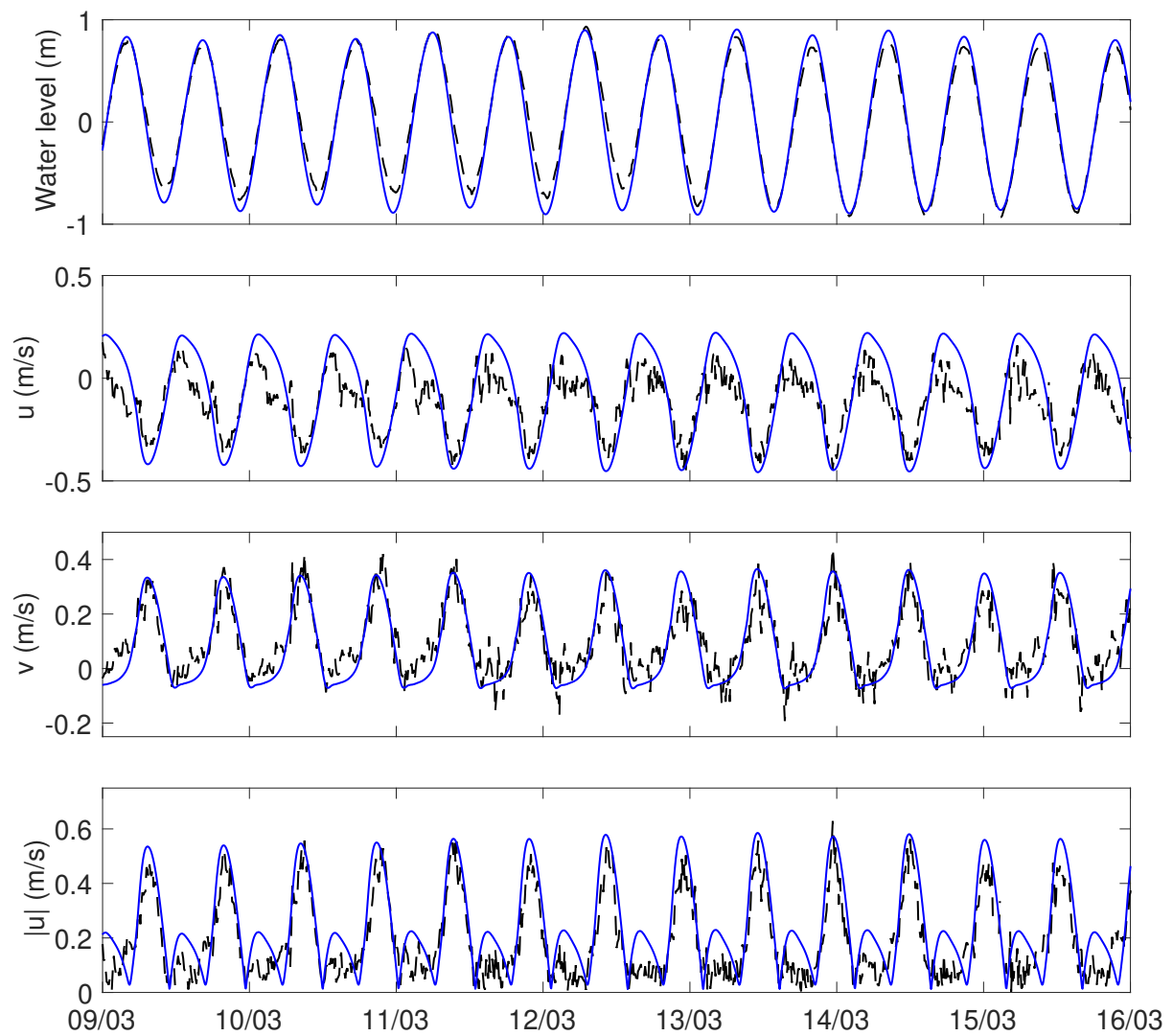


**Figure A1.1.** Calibration plots of measured (black dashed line) and modelled (solid blue line) water levels, current speeds, U velocities (east) and V velocities (north) from site #2 (Figure 3).

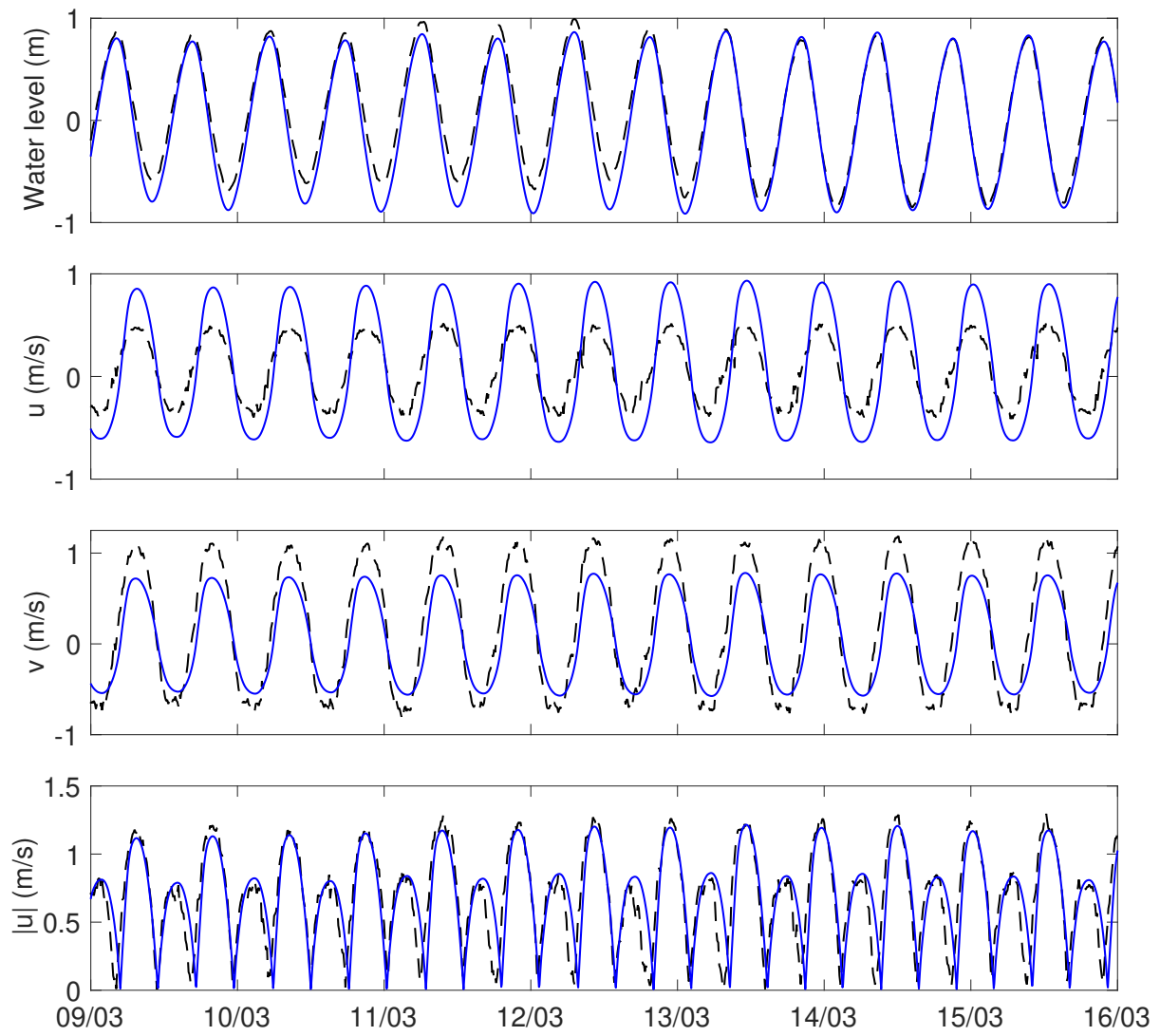


**Figure A1.2.** Calibration plots of measured (black dashed line) and modelled (solid blue line) water levels, current speeds, U velocities (east) and V velocities (north) from site #3 (Figure 3).

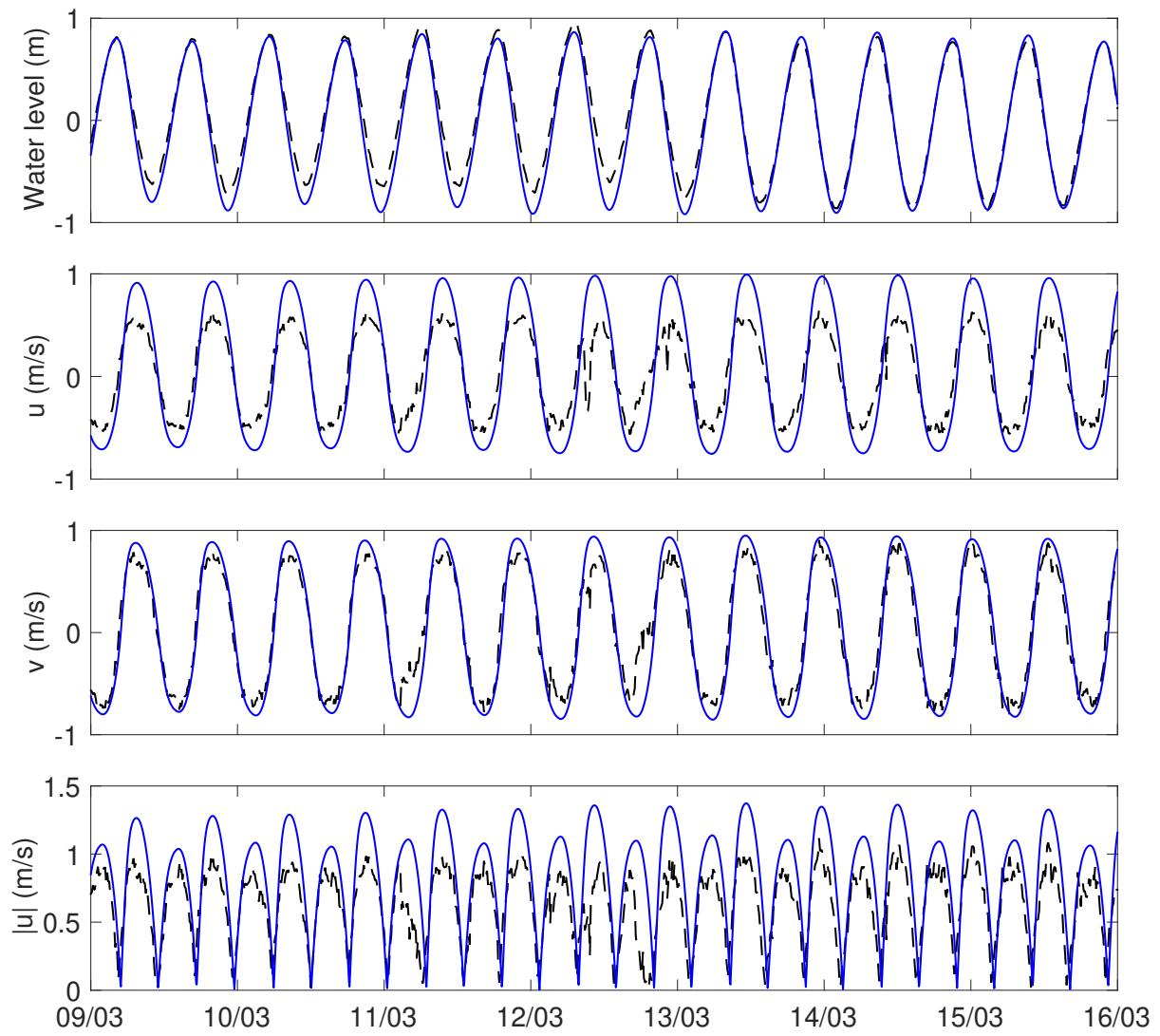


**Figure A1.3.** Calibration plots of measured (black dashed line) and modelled (solid blue line) water levels, current speeds, U velocities (east) and V velocities (north) from site #4 (Figure 3).

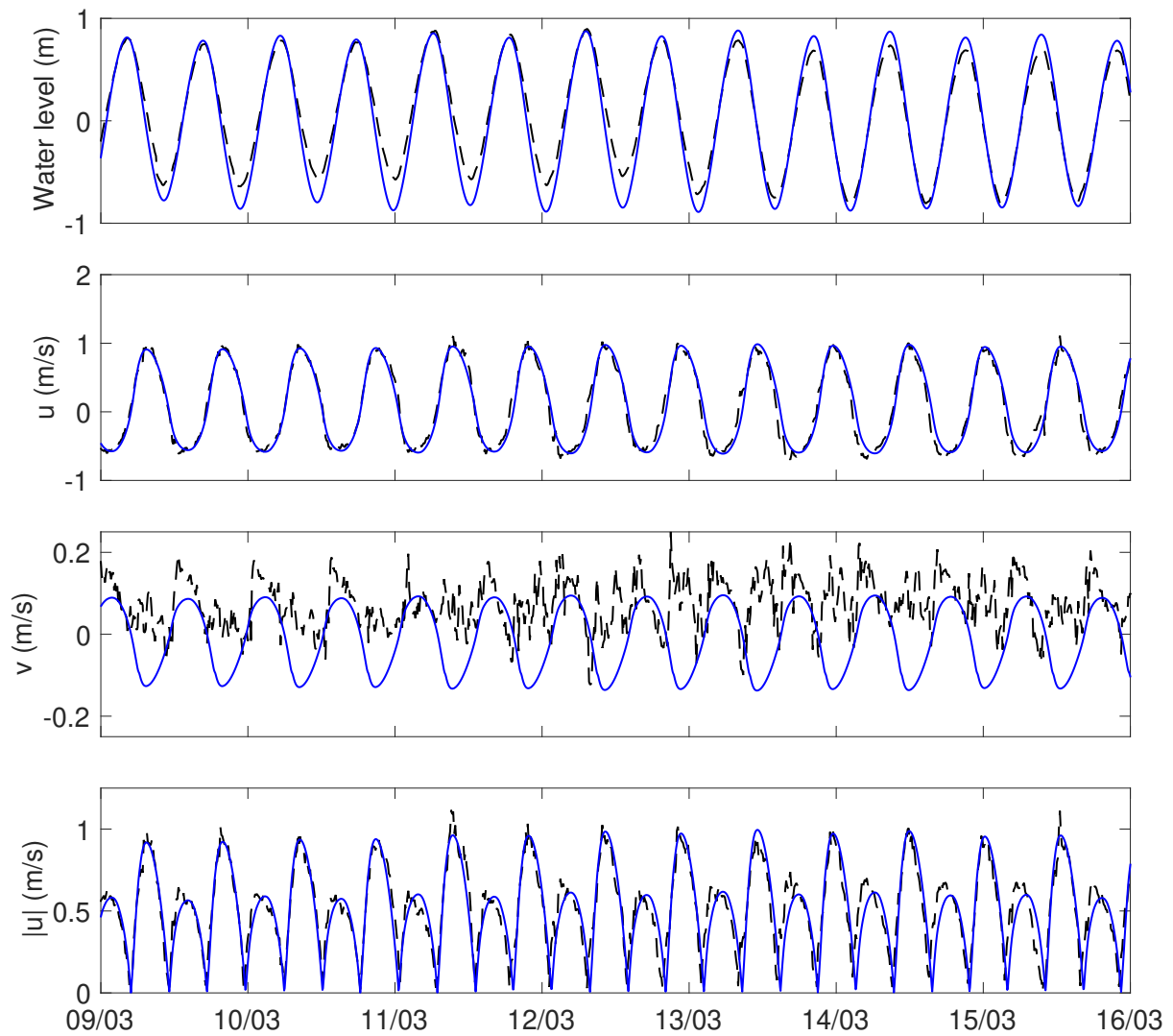


**Figure A1.4.** Calibration plots of measured (black dashed line) and modelled (solid blue line) water levels, current speeds, U velocities (east) and V velocities (north) from site #5 (Figure 3).

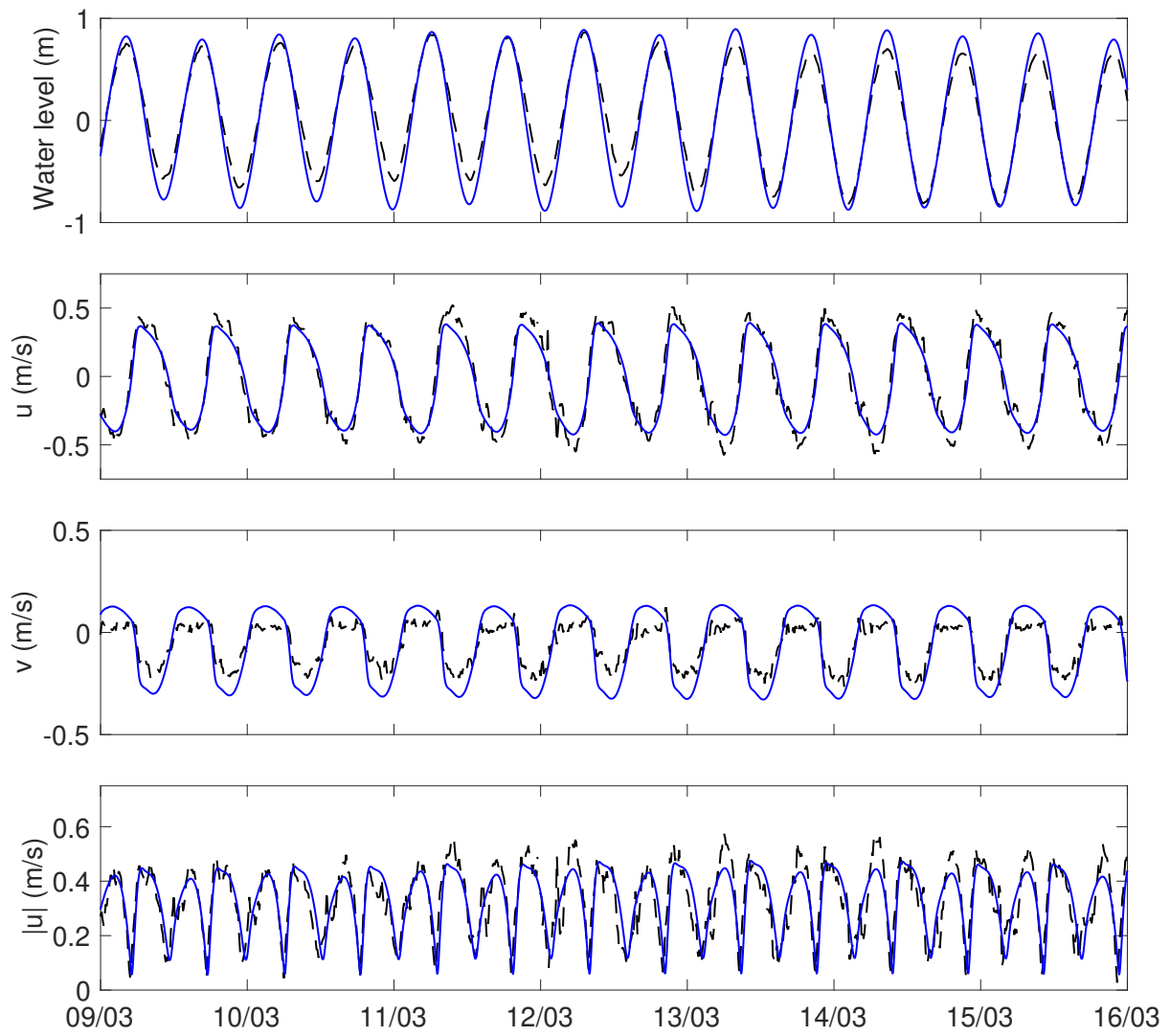


**Figure A1.5.** Calibration plots of measured (black dashed line) and modelled (solid blue line) water levels, current speeds, U velocities (east) and V velocities (north) from site #6 (Figure 3).

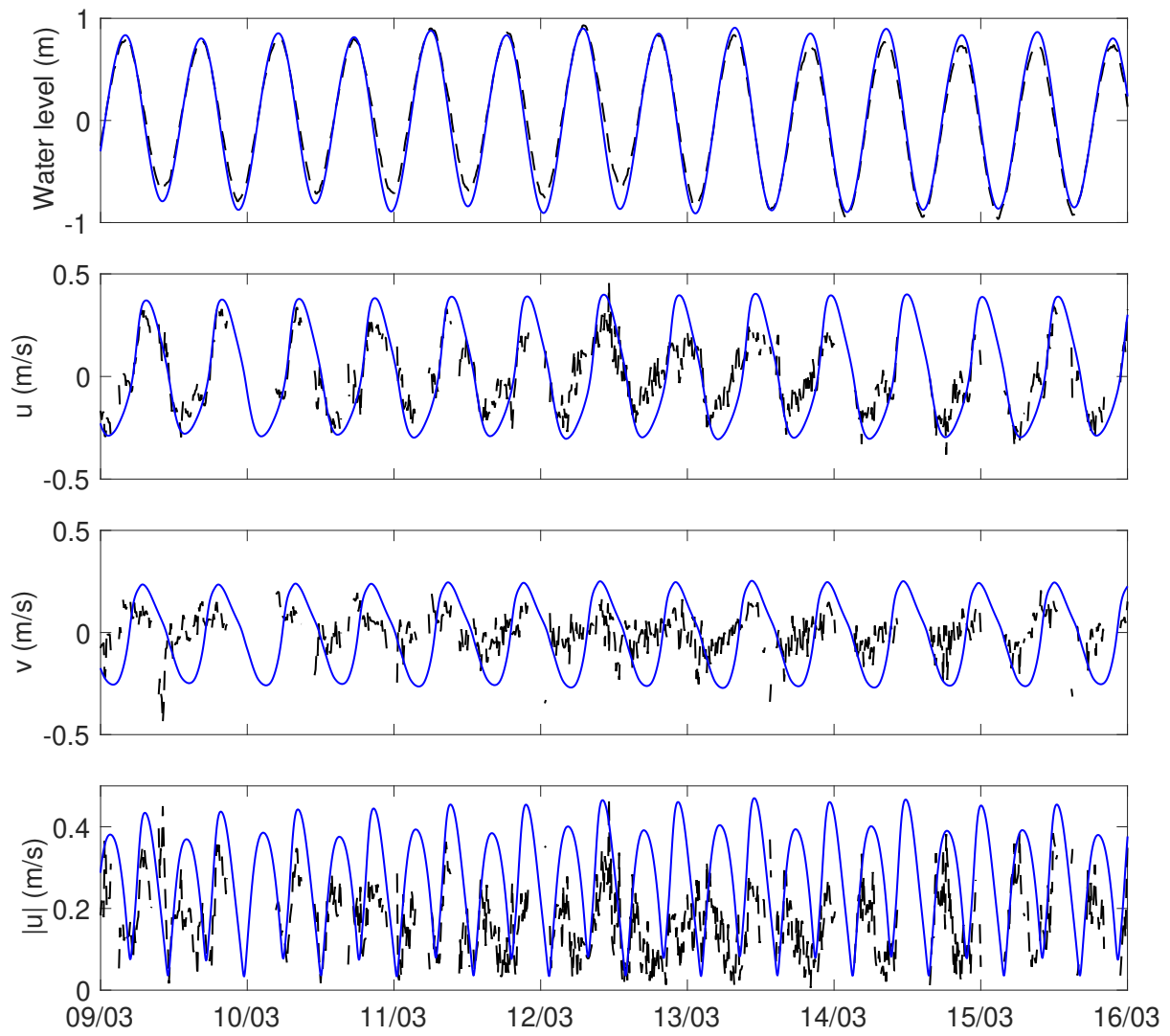


**Figure A1.6.** Calibration plots of measured (black dashed line) and modelled (solid blue line) water levels, current speeds, U velocities (east) and V velocities (north) from site #7 (Figure 3).

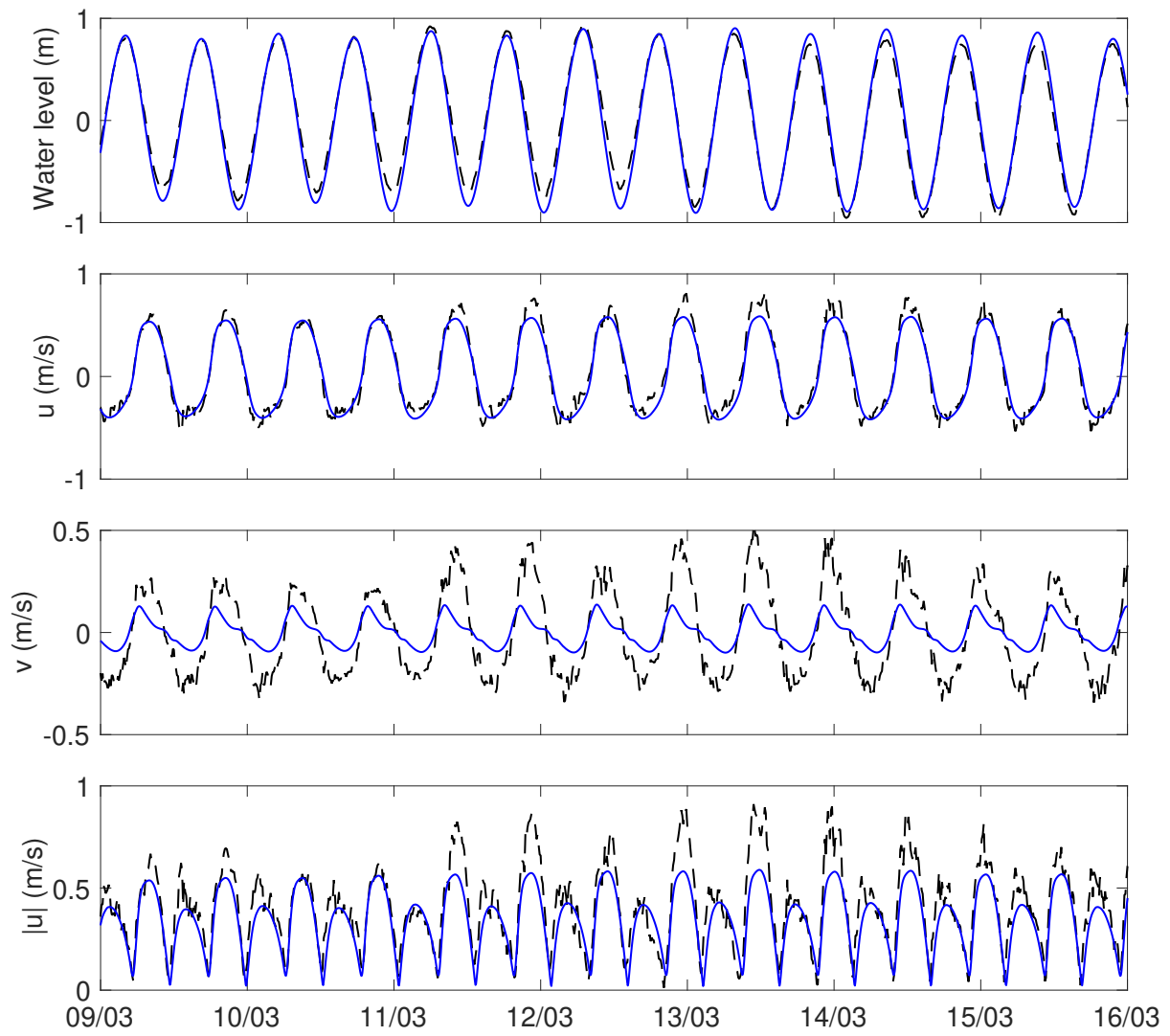


**Figure A1.7.** Calibration plots of measured (black dashed line) and modelled (solid blue line) water levels, current speeds, U velocities (east) and V velocities (north) from site #8 (Figure 3).

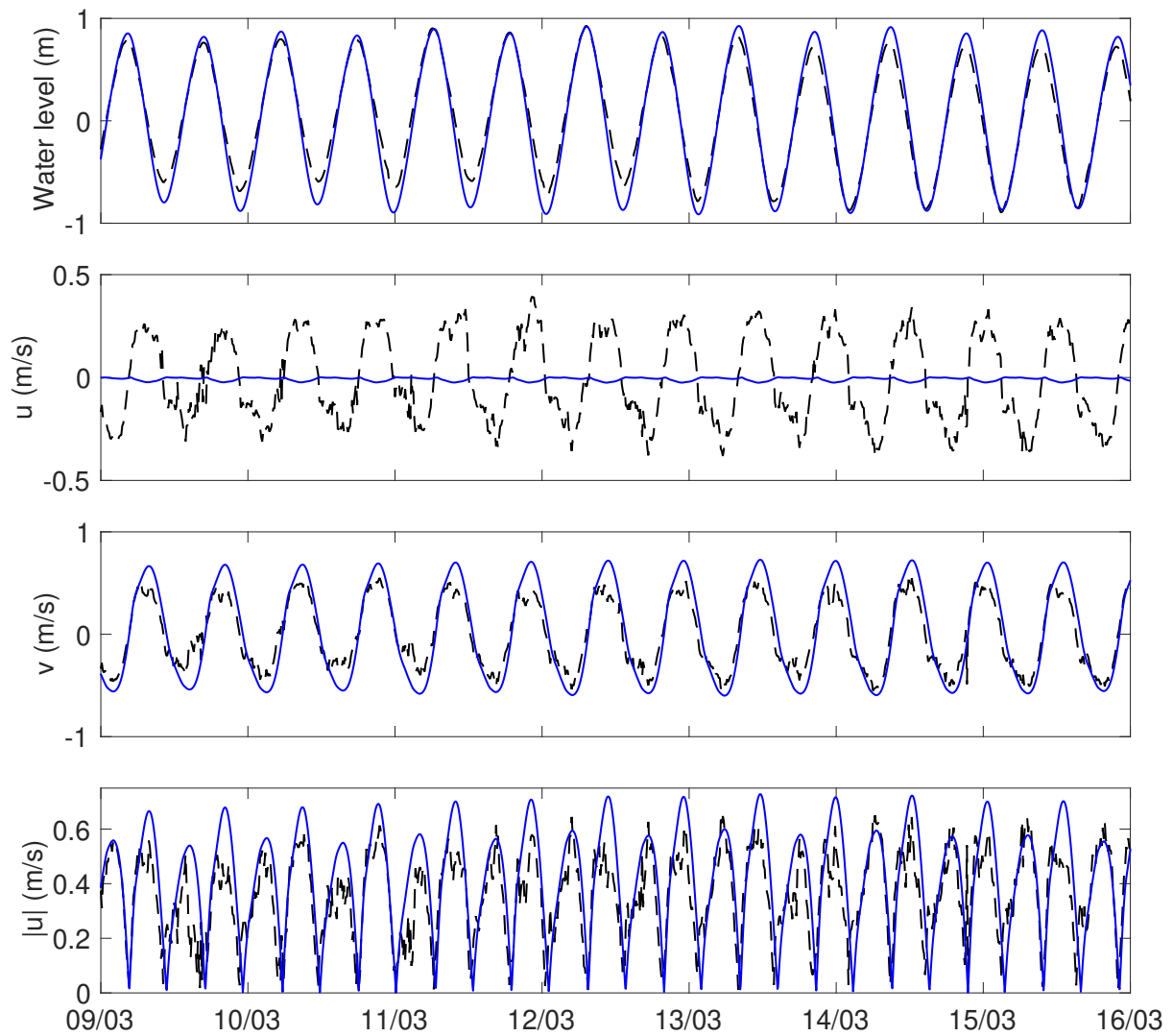


**Figure A1.8.** Calibration plots of measured (black dashed line) and modelled (solid blue line) water levels, current speeds, U velocities (east) and V velocities (north) from site #9 (Figure 3).